Electron densities and related properties from the *ab-initio* simulation of crystalline solids

Cesare Pisani, Roberto Dovesi, Alessandro Erba and Paolo Giannozzi

February 9, 2010

Abstract This chapter deals with the charge, spin and momentum densities of electrons in crystalline solids as obtained from *ab-initio* simulations. It describes state-of-the-art approaches using plane waves or local basis functions, and comments on their main advantages and drawbacks. The influence of computational parameters on densities is demonstrated by way of examples. Ongoing developments are briefly discussed: thermal effects, response to external perturbations, post-Hartree Fock treatment of electron correlation.

1 Introduction

The aim of this chapter is to provide a general introduction to the *ab-initio* simulation of the density matrix (DM) of crystalline systems, and derived functions: charge, spin and momentum densities generally indicated as "density functions (DF)", and to describe by way of examples the performance of state-of-the-art computational tools in this respect.

Table 1 sketches possible standards of quality which may be pursued. Stepping down from one level to that below corresponds to missing some aspects of the phys-

Cesare Pisani
Dipartimento di Chimica IFM, and Centre of Excellence NIS (Nanostructured Interfaces and Surfaces), Università di Torino, via Giuria 5, I-10125 Torino (Italy) e-mail: cesare.pisani@unito.it

Roberto Dovesi
Dipartimento di Chimica IFM, and Centre of Excellence NIS (Nanostructured Interfaces and Surfaces), Università di Torino, via Giuria 5, I-10125 Torino (Italy) e-mail: roberto.dovesi@unito.it

Alessandro Erba
Dipartimento di Chimica IFM, and Centre of Excellence NIS (Nanostructured Interfaces and Surfaces), Università di Torino, via Giuria 5, I-10125 Torino (Italy) e-mail: alessandro_erba@virgilio.it

Paolo Giannozzi
CNR-INFM Democritos National Simulation Center, I-34151 Trieste (Italy) and Dipartimento di Fisica, Università di Udine, via delle Scienze 208, I-33100 Udine (Italy) e-mail: paolo.giannozzi@uniud.it

Table 1 Different levels of approximation in the theoretical simulation (see text for comments).

Level 0:	Complete "ensemble" description of the system		
	Relativistic effects: core contraction, spin-orbit coupling, etc.	Effects of external fields	Coupling of nuclear and electronic motions; thermal effects
Level 1:	Non-relativistic description of electronic ground-state at fixed-nuclei equilibrium configuration		
		Instantaneous correlation of electronic motions	
Level 2:	Single-determinantal HF or KS description of electronic ground-state		
	Selection of exchange-correlation KS potential	Selection of representative BS	Algebraic solution of HF or KS equations within selected BS
Level 3:	Approximate HF or KS description of electronic ground-state		

ical description of the problem, and/or to adopting some simplifying assumptions as specified in the framed boxes in between.

We shall take as the center of our treatment the level marked "1" in that table, that is, our reference *exact* DM and DFs will be those obtained from the ground-state solution of the Schrödinger equation in the absence of external fields:

$$\widehat{H}_{\rm el}\,\Psi_0 \;=\; E_0\,\Psi_0 \tag{1}$$

In Section 2 the formalism is introduced. In Subsection 2.1 we define the exact DM and DFs for periodic structures, establish their relationship with the *ideal* experimental observables, and derive some general facts about them. The very fact that we are interested in "infinite" systems, makes the solution of equation (1) practically impossible at the present state-of-the-art of computational techniques, in spite of the simplifying constraint of translational symmetry. In order to obtain useful results,

we are forced to adopt an "average-field" approximation of the electrostatic Hamiltonian that is, to step down to level 2 of table 1, using either a Hartree-Fock (HF), or a Kohn-Sham (KS) approach. In Subsection 2.2 these one-electron schemes are considered. The general aspects of the corresponding single-determinant wavefunctions are reviewed, and some peculiar properties of the resulting DM and DFs are recalled. Specific problems related with the treatment of core electrons (the possible use of pseudopotentials, the need for relativistic corrections) are briefly discussed.

Of course, substantial effort and computational approximations are required even for obtaining a reasonable description of the single-determinantal solution of our problem. In practice, we are working at level 3 of table 1, and our main aim will be to assess the importance of computational parameters in determining the distance with respect to level 2 quantities. Section 3 discusses explicitly the schemes of solution which are most commonly adopted for this case. It is shown that the very structure of the code and the technical peculiarities are to a large extent determined by the basis set (BS) adopted, either plane waves (PW) or local functions attached to the nuclei, conventionally indicated as atomic orbitals (AO). To be more specific, two codes are illustrated in some detail, Quantum ESPRESSO [1] and CRYSTAL [2], which adopt PWs and AOs respectively. It is only fair to state that a number of excellent periodic programs exist nowadays which are in widespread use in the scientific community (reference to some of them is provided in [3]). However, the fact that the Authors of this Chapter are among the developers of those two codes has permitted them to go deeper into the analysis of the effect of the various computational parameters on the quality of the resulting DM. As a matter of fact, this kind of analysis is relatively new, since the primary (often exclusive) object of interest for developers and users of the codes is the total energy of the system. On the other hand, this quantity is of fundamental importance also in the present context because it determines factors such as equilibrium geometries, pressure effects and normal vibrational modes, which directly affect calculated DFs.

Section 4 considers precisely by way of examples the influence of computational parameters (including the special form of the one-electron Hamiltonian and the BS) on charge, spin, momentum densities. Some simple systems are considered which cover a wide variety of electronic structures and types of bonding; for each of them a few selected aspects are analyzed in depth.

Once we have reached a solution close to our level-2 objective, it is worth trying to look back at the higher levels of the ladder of table 1, in order to see what information has been missed, and possibly to partly recover it. Three aspects will be considered for this purpose in Section 5, with reference to ongoing research. In the first instance, the harmonic description of nuclear motions is shown to allow a statistical estimate of zero-point and thermal effects on DFs. Secondly, we discuss how to study the modifications induced by the presence of external fields. Thirdly, the *ab-initio* re-introduction of instantaneous electron correlation that is, the upgrade from level 2 to level 1, is entering into the realm of feasibility even for periodic systems, and it may be interesting to understand how much this aspect may influence DFs.

Some general conclusions are tentatively drawn in Section 6.

2 The theoretical frame

As anticipated in the Introduction, our reference level requires the solution of equation (1), where the non-relativistic electrostatic Hamiltonian for the N-electron system in the fi eld of M nuclei of charge Z_A at $\mathbf{R}_A$ is given by the following expression:

$$\widehat{H}_{\rm el} = \sum_{n=1}^{N} \frac{-\nabla_n^2}{2} + \sum_{n=1}^{N} \sum_{A=1}^{M} \frac{-Z_A}{r_{nA}} + \frac{1}{2} {\sum_{n,m=1}^{N}}' \frac{1}{r_{nm}} + \frac{1}{2} {\sum_{A,B=1}^{M}}' \frac{Z_A Z_B}{r_{AB}} \qquad (2)$$

Atomic units (au) are here used (see Appendix); the primed double sums exclude "diagonal" terms ($n = m$, $A = B$). $\widehat{H}_{\rm el}$ depends parametrically on the sets $\{\mathbf{R}\}, \{Z\}$ of the positions $\mathbf{R_A}$ and charges Z_A of the M nuclei, so the same is true for E_0, Ψ_0.

Ψ_0 is an antisymmetric function of the space-spin coordinates $\mathbf{x}_n \equiv \mathbf{r}_n, \sigma_n$ of the N electrons ($n = 1, \ldots, N$). The nuclear coordinates for which $E_0[\{\mathbf{R}\}, \{Z\}]$ has its minimum $E_0^{\rm eq}$ will be labelled $\{\mathbf{R}^{\rm eq}\}$. The corresponding eigenfunction, $\Psi_0^{\rm eq}$, can then be written as follows:

$$\Psi_0^{\rm eq}(\ldots, \mathbf{x}_n, \ldots) \equiv \Psi_0(\ldots, \mathbf{x}_n, \ldots; [\{\mathbf{R}^{\rm eq}\}, \{Z\}]) \qquad (3)$$

The special case of neutral periodic systems is the only one that will be treated here. Consider a lattice of vectors $\mathbf{T_m}$ generated starting from D primitive linearly independent *basis vectors* $\mathbf{a}_i$ of ordinary space:

$$\mathbf{T_m} = \sum_{i=1}^{D} m_i \mathbf{a}_i \qquad (4)$$

where m_i are integers, and D is the number of periodic directions (three for bulk crystals, two for slabs, one for polymeric structures). The $\mathbf{a}_i$ vectors defi ne (not univocally) the *unit cell* of the crystal. It is assumed that the coordinates and charges of all nuclei can be generated from those of a translationally irreducible fi nite set $\{\mathbf{R}_{A,\mathbf{0}}\,;\, Z_{A,\mathbf{0}}\}$ as follows:

$$\mathbf{R}_{A,\mathbf{m}} = \mathbf{R}_{A,\mathbf{0}} + \mathbf{T_m} \quad ; \quad Z_{A,\mathbf{m}} = Z_{A,\mathbf{0}} \qquad (5)$$

For the solution of equation (1), the Born-von Kármán (BvK) cyclic conditions will be adopted. They correspond to assuming that Ψ_0 is cyclically periodic with respect to a super-lattice of vectors $\overline{\mathbf{W}}_\mathbf{m}$ defi ned as in equation (4), but starting from D *super-basis vectors* $\overline{\mathbf{A}}_i = w_i \mathbf{a}_i$:

$$\begin{aligned} &\text{if:} \quad \mathbf{x}_n = (\mathbf{r}_n, \sigma_n)\,,\ \mathbf{x}'_n = (\mathbf{r}_n + \overline{\mathbf{W}}_\mathbf{m}, \sigma_n)\,, \\ &\text{then:} \quad \Psi_0(\ldots, \mathbf{x}_n, \ldots) = \Psi_0(\ldots, \mathbf{x}'_n, \ldots) \qquad \forall\, n, \mathbf{m} \qquad \{\text{BvK}\} \end{aligned} \qquad (6)$$

(here and in the following $\{\text{BvK}\}$ labels relationships that hold true owing to BvK conditions). The integers w_i defi ne the *effective number* of electrons in the system: $N^{\rm eff} = W N_0$, with $W = \prod_i w_i$, and $N_0 = \sum_A Z_{A,\mathbf{0}}$ the number of electrons per cell.

Provided the w_i's are large enough (see Section 3.1), their choice is scarcely influential on the quality of the results as concerns energy dependent quantities. On the other hand, account must be taken of the effect of the BvK conditions on DM and DFs in order to avoid misinterpretation of the results (see for instance equation 23).

2.1 Definition and properties of exact DM and DFs

Following McWeeny [4], we can define the one-particle generalized density function, our exact *position-spin* DM, as follows (by default, $\Psi_0 = \Psi_0^{\mathrm{eq}}$):

$$\gamma(\mathbf{x};\mathbf{x}') \;=\; N \int \Psi_0(\mathbf{x},\mathbf{x}_2,\ldots,\mathbf{x}_N) \times \big(\Psi_0(\mathbf{x}',\mathbf{x}_2,\ldots,\mathbf{x}_N)\big)^* \,\mathrm{d}\mathbf{x}_2 \ldots \mathrm{d}\mathbf{x}_N \qquad (7)$$

Higher-order DMs can be usefully defined, but they don't matter in the present context. The content of information of $\gamma(\mathbf{x};\mathbf{x}')$ is very rich. This function of only six spatial and two spin coordinates provides the ground-state expectation value of any observable described by a one-electron operator $\widehat{F} = \sum_n \hat{f}[\mathbf{x}_n]$:

$$\langle\, \widehat{F} \,\rangle_0 = \int \big\{ \hat{f}[\mathbf{x}]\, \gamma(\mathbf{x};\mathbf{x}') \big\}_{(\mathbf{x}'=\mathbf{x})} \,\mathrm{d}\mathbf{x} \qquad (8)$$

By making explicit the dependence of $\gamma(\mathbf{x};\mathbf{x}')$ on the two-valued spin coordinates with respect to the z direction $[\sigma,\sigma' = \alpha,\beta]$, we can define the *spin-projected components* of the DM:

$$\begin{gathered} P^{\sigma}(\mathbf{r};\mathbf{r}') \;=\; \gamma(\mathbf{r},\sigma;\mathbf{r}',\sigma) \\ P(\mathbf{r};\mathbf{r}') = P^{\alpha}(\mathbf{r};\mathbf{r}') + P^{\beta}(\mathbf{r};\mathbf{r}') \;\;;\;\; Q(\mathbf{r};\mathbf{r}') = P^{\alpha}(\mathbf{r};\mathbf{r}') - P^{\beta}(\mathbf{r};\mathbf{r}') \end{gathered} \qquad (9)$$

$P(\mathbf{r};\mathbf{r}')$ is called the *position* DM, obtained by integrating $\gamma(\mathbf{x};\mathbf{x}')$ over both spin components, while $Q(\mathbf{r};\mathbf{r}')$ is the *excess DM* of α- with respect to β-electrons.

The *momentum* DM is the six-dimensional Fourier transform (FT) of $P(\mathbf{r};\mathbf{r}')$:

$$\overline{P}(\mathbf{p};\mathbf{p}') = \int P(\mathbf{r};\mathbf{r}') \exp(-\imath\mathbf{r}\cdot\mathbf{p}) \exp(\imath\mathbf{r}'\cdot\mathbf{p}')\,\mathrm{d}\mathbf{r}\,\mathrm{d}\mathbf{r}' \qquad (10)$$

DFs are the "diagonal elements" of the DMs:

$$\begin{aligned} \rho(\mathbf{r}) \;&=\; P(\mathbf{r};\mathbf{r}) && \textbf{electron density (ED)} \\ \rho^{\sigma}(\mathbf{r}) \;&=\; P^{\sigma}(\mathbf{r};\mathbf{r}) && \textbf{electron } \sigma\textbf{-spin density} \\ \zeta(\mathbf{r}) \;&=\; Q(\mathbf{r};\mathbf{r}) = \rho^{\alpha}(\mathbf{r}) - \rho^{\beta}(\mathbf{r}) && \textbf{electron (net) spin density (ESD)} \text{ (along } z\text{)} \\ \pi(\mathbf{p}) \;&=\; \overline{P}(\mathbf{p};\mathbf{p}) && \textbf{electron momentum density (EMD)} \end{aligned} \qquad (11)$$

They are *observable quantities* in a quantum-mechanical sense, since they are the ground-state expectation value of one-electron operators $[\widehat{F}^{\mathbf{y}} = \sum_n \delta(\mathbf{y} - \mathbf{y}_n)]$.

In a periodic system, the displacement of *all* $\mathbf{r}_n$ quantities by the same lattice vector $\mathbf{T}_m$ must just result in a change of the ground state wavefunction by a phase factor. From equation (7) we then have:

$$\gamma(\mathbf{r},\sigma;\mathbf{r}',\sigma') = \gamma(\mathbf{r}+\mathbf{T}_m,\sigma;\mathbf{r}'+\mathbf{T}_m,\sigma') \; ; \; P(\mathbf{r};\mathbf{r}') = P(\mathbf{r}+\mathbf{T}_m;\mathbf{r}'+\mathbf{T}_m) \quad (12)$$

All information about the position(-spin) DMs is thus obtained by confi ning the variable $\mathbf{r}$ to within the unit cell. In equation (10), the integral over $\mathbf{r}$ can then be limited to the unit cell. With this convention, which makes $\pi(\mathbf{p})$ independent of the "size" of the crystal: $\int \pi(\mathbf{p})\mathrm{d}\mathbf{p} = N_0$, the number of electrons per cell.

The BvK conditions (equation 6) entail a stronger consequence on DMs:

$$\gamma(\mathbf{r},\sigma;\mathbf{r}',\sigma') = \gamma(\mathbf{r},\sigma;\mathbf{r}'+\overline{\mathbf{W}}_m,\sigma') \; ; \; P(\mathbf{r};\mathbf{r}') = P(\mathbf{r};\mathbf{r}'+\overline{\mathbf{W}}_m) \quad \{\mathrm{BvK}\} \quad (13)$$

It is not our concern to discuss explicitly how information on these observables can be obtained from actual experiments: this question is dealt with elsewhere in this Book. But while commenting below on some general properties of the exact DFs, with special attention to the consequences of translational periodicity, we will also establish their relationship with "ideal" measurable quantities such as structure factors, Compton profi les, etc.

Chapter 6 provides a more complete analysis of the relationships among the various DMs and DFs, and between these and the chemical characteristics of the system.

2.1.1 Electron density

In many respects, the ED $\rho(\mathbf{r})$ (also called electron charge density, ECD) and its spin components have the same properties; we consider here only the former quantity while we shall discuss some aspects of the ESD $\zeta(\mathbf{r})$ in Section 4.

$\rho(\mathbf{r})$ plays a specially important role in the characterization of the many-electron system. This is a simple function of the space coordinates (it is real, non-negative, fi nite everywhere and regular except for isolated cusps) which reflects faithfully the chemical composition and geometry of the system. In fact, the position $\mathbf{R}_A$ and the charge Z_A of all the nuclei are identifi ed, respectively, through the location of the cusps and through the Kato's cusp condition [5]: $Z_A = -\overline{\rho'(\mathbf{R}_A)}/(2\,\rho(\mathbf{R}_A))$, where $\overline{\rho'(\mathbf{R}_A)}$ is the spherical average of the slope about the cusp. It therefore contains transparently all information about the Schrödinger Hamiltonian of the system. The recognition of this fact, although derived differently [6], is at the basis of density functional theory (DFT) which has enjoyed enormous success especially in its KS formulation [7] (see Subsection 2.2).

Bader's Atoms in Molecules theory [8] and its application to crystals [9, 10] allows a wealth of information about the chemical features of the system to be obtained through a topological analysis the ED and its derivatives (see Chapter 1). Recent literature concerning the comparison between experimental and theoretical ED determinations is in fact often centered on the respective characterization of Bader's topological objects, in particular of the bond critical points [11].

Since a non-degenerate ground-state wavefunction [hence the corresponding $\rho(\mathbf{r})$] has the same symmetry as the Hamiltonian, the ED of a crystalline system is invariant to all operations of the related space group $\mathscr{S}$:

$$\{V \mid T_{\mathbf{m}} + \mathbf{s}_V\}\,\rho(\mathbf{r}) \equiv \rho(V^{-1}\mathbf{r} - T_{\mathbf{m}} - \mathbf{s}_V) = \rho(\mathbf{r}) \tag{14}$$

The Seitz notation of the operators has been used [12], where V is a matrix representing a proper or improper rotation, and $\mathbf{s}_V$ the associated fractional translation (for the so-called symmorphic groups, $\forall V:\ \mathbf{s}_V = \mathbf{0}$). The rotations themselves form a group of order h, the *point group of the crystal*. Because of equation (14), all information about the ED is contained in a $1/h$-th wedge of the unit cell (the irreducible wedge). Integration of $\rho(\mathbf{r})$ over the irreducible wedge gives N_0/h.

A one-to-one correspondence exists between the ED and its 3-dimensional FT, the *form factor*:

$$F(\boldsymbol{\kappa}) = \int \rho(\mathbf{r}) \exp(\imath\,\boldsymbol{\kappa}\cdot\mathbf{r})\,\mathrm{d}\mathbf{r} \tag{15}$$

Let us associate to the D unit vectors of direct lattice, $\mathbf{a}_i$, an equal number of unit vectors of reciprocal lattice, $\mathbf{B}_j$ defi ned by the relation: $\mathbf{a_i}\cdot\mathbf{B}_j = 2\pi\delta_{ij}$ $(i, j = 1, \ldots, D)$. The general point of reciprocal space can then be written as a sum of a "periodic part": $\boldsymbol{\kappa}^{\parallel} = \sum_{i=1}^{D} \kappa_i\,\mathbf{B_i}$, and of a "non-periodic part", $\boldsymbol{\kappa}^{\perp}$, perpendicular to the former. The symmetry properties of the ED (equation 14) entail the following consequences for the crystalline form factor (the case D=3 is considered for defi niteness, where $\boldsymbol{\kappa} \equiv \boldsymbol{\kappa}^{\parallel}$):

1. Due to translational invariance, $F(\boldsymbol{\kappa})$ is zero unless $\boldsymbol{\kappa}$ is a *reciprocal lattice vector* $\mathbf{G}_{hkl} \equiv h\mathbf{B}_1 + k\mathbf{B}_2 + l\mathbf{B}_3$, with h, k, l integers. The form factor is then defi ned by the discrete (but infi nite) set of the *structure factors*:

$$F_{hkl} = \int_{\text{unit cell}} \rho(\mathbf{r}) \exp(\imath\,\mathbf{G}_{hkl}\cdot\mathbf{r})\,\mathrm{d}\mathbf{r} \tag{16}$$

   By this convention, structure factors are normalized so that $F_{000} = N_0$, the number of electrons in the (conventional) crystallographic unit cell.
2. Due to rotational invariance, $F(\mathbf{G}) = \exp(-\imath\mathbf{G}\cdot\mathbf{s}_V)\,F(V\mathbf{G})$: that is, F_{hkl} is the same up to a phase factor for reciprocal lattice vectors which are obtained from each other by a point group operation (belong to the same *star*).
3. Depending on the space group, some structure factors are systematically zero (*"general" extinction conditions*); *"extra" extinction conditions* may apply to the triplet *hkl*, when $\rho(\mathbf{r})$ can be expressed as a sum of contributions from "spherical" atoms centered in some special Wyckoff positions: see e.g. reference [13].

In the dynamical limit and in the hypothesis of fi xed nuclei, the X-ray structure factors provided by diffraction experiments are the *ideal* experimental counterpart of the theoretical ones. When trying to reconstruct EDs from actual diffraction data, apart from all the corrections that must be applied for obtaining a guess of the ideal structure factors [11], a *phase factor* problem exists since only the modulus of the latter is provided by the experiment. The comparison (Theory) $\longrightarrow$ (Experiment)

as concerns EDs is then more natural than the reciprocal one, because a number of corrections can easily be applied to the theoretical structure factors (including approximate account of nuclear thermal motion, see Section 5.1), so as to make the comparison with their experimental counterpart as justified as possible.

2.1.2 Momentum density

The electron momentum density (EMD), $\pi(\mathbf{p})$, brings in complementary information with respect to the ED, as is discussed at length in Chapter 6. In particular, the features of $\pi(\mathbf{p})$ near the origin are dominated by the contributions of the slow valence electrons, while those at large $|p|$ values reflect the properties of core electrons. The convention introduced at the beginning of this Section is adopted, according to which $\pi(\mathbf{p})$ in a crystal is normalized to N_0, the number of electrons per cell. Some basic facts about the EMD are here recalled.

$\pi(\mathbf{p})$ is a real, positive definite function which exhibits rotational invariance with respect to all operators of the point group of the crystal $[\pi(\mathbf{p}) = \pi(V\mathbf{p})]$.

It provides directly the ground-state expectation value of the total kinetic energy per cell of the electrons in the system:

$$\langle \widehat{T} \rangle_0 = \frac{1}{2} \int \pi(\mathbf{p})\, p^2 \, \mathrm{d}\mathbf{p} \tag{17}$$

Due to the virial theorem, which holds true for the electrostatic Hamiltonian of equation (2), the EMD also provides the total energy per cell at the equilibrium configuration:

$$\frac{1}{2} \int \pi(\mathbf{p})_{(\{\mathbf{R}\}=\{\mathbf{R}^{\mathrm{eq}}\})}\, p^2 \, \mathrm{d}\mathbf{p} = -E_0^{\mathrm{eq}} \tag{18}$$

This important relationship, which derives from minimization of the expectation value of energy with respect to the scaling of *all* coordinates, is *not* valid in more general cases, for instance for volume-constrained optimized configurations.

Two interesting functions can be obtained from the EMD: the *Reciprocal Form Factor* (RFF), $B(\mathbf{r})$, and the *Compton Profile Function* (CPF), $J(\mathbf{q})$:

$$\begin{aligned} B(\mathbf{r}) &= \int \pi(\mathbf{p}) \exp(-\imath \mathbf{p}\cdot\mathbf{r}) \, \mathrm{d}\mathbf{p} = \frac{1}{W} \int P(\mathbf{r}';\mathbf{r}+\mathbf{r}') \, \mathrm{d}\mathbf{r}' \\ J(\mathbf{q}) &= \int \pi(\mathbf{p})\, \delta\left(\frac{\mathbf{p}\cdot\mathbf{q}}{|\mathbf{q}|} - |\mathbf{q}| \right) \mathrm{d}\mathbf{p} \end{aligned} \tag{19}$$

The two definitions of the RFF are easily seen to be equivalent; the second one justifies its alternative name of *Autocorrelation Function*. The normalizing factor W is the number of cells in the cyclic crystal; we then have, as expected: $B(\mathbf{0}) = N_0$.

The CPF results from the 2-D integration of $\pi(\mathbf{p})$ over a plane through $\mathbf{q}$ perpendicular to the $\mathbf{q}$ direction. Its main interest stems from the fact that it can be related to the *ideal* experimental Compton profiles (CP) [14]. Consider the *directional* CP:

$$J_{hkl}(q) = J(q\,\mathbf{e}_{hkl}) \qquad \left(\mathbf{e}_{hkl} = \frac{h\mathbf{a}_1 + k\mathbf{a}_2 + l\mathbf{a}_3}{|h\mathbf{a}_1 + k\mathbf{a}_2 + l\mathbf{a}_3|}\right) \tag{20}$$

In the sudden-impulse approximation, this function is proportional to the distribution of the loss, in the direction $\mathbf{e}_{hkl}$, of the momentum of scattered photons, as is measured in a Compton scattering experiment.

The *directional* RFF [$B_{hkl}(s) = B(s\mathbf{e}_{hkl})$] and the corresponding directional CP are immediately seen to be related to each other by a *one-dimensional* FT:

$$B_{hkl}(s) = \int J_{hkl}(q)\, \exp(-\imath sq)\, \mathrm{d}q \tag{21}$$

An interesting consequence of this relation can be cited. Due to limited resolution, experimental directional CPs [$J^{\mathrm{exp}}_{hkl}(q)$] can be considered as the *convolution* of the ideal CP by the experimental resolution function $w(q)$ (usually a Gaussian):

$$J^{\mathrm{exp}}_{hkl}(s) \approx \int J_{hkl}(q')\, w(q' - q)\, \mathrm{d}q' \tag{22}$$

It then follows that $B_{hkl}(s)$ is simply the FT of $J^{\mathrm{exp}}_{hkl}(q)$ *divided by* $\overline{w}(s)$, the FT of $w(q)$. The RFF is therefore easily accessible from the Compton scattering experiment. Furthermore, its fine structure is not affected very much by experimental errors; in particular its zeros can be located with relatively high precision.

A consequence of the BvK conditions on the calculated RFF can be noted: from equation (13) it immediately follows that the latter has (artificially) the periodicity of the superlattice:

$$B(\mathbf{r}) = B(\mathbf{r} + \overline{\mathbf{W}}_{\mathbf{m}}) \qquad \{\mathrm{BvK}\} \tag{23}$$

The RFF conveys important information. Its oscillatory behaviour in direct space, the position of its nodal surfaces, the value of its maxima and minima are closely related to the chemical features of the system [15]: these topics are treated in detail in Chapter 6 of this book.

2.2 HF and KS schemes, and related DM and DFs

The solution of equation (1) that is, the determination of the eigenfunction Ψ_0, is impossible for any system of real interest. Two simplified schemes, HF and KS, are usually adopted for describing periodic systems, which may provide valuable information on their DMs and DFs. Here we consider their exact formulation, and comment on some characteristic aspects of the resulting densities; in Section 3, we shall describe their actual implementation and the simplifying assumptions which must be adopted in order to obtain their approximate solution.

HF and KS have many features in common. In their *spin-unrestricted* formulation (UHF,UKS), both are intended to obtain a set of N one-electron functions, the *molecular spin-orbitals* (MSO) (or *crystalline spin-orbitals*, CSO, in the periodic

case), $\psi_j^{\mathrm{X}}(\mathbf{x}) = \phi_j^{\mathrm{X},\sigma}(\mathbf{r})\omega(\sigma)$, with σ either α or β, which satisfy the equation:

$$\hat{h}^{\mathrm{X},\sigma}\phi_j^{\mathrm{X},\sigma}(\mathbf{r}) = \left[-\frac{\nabla^2}{2} + \sum_A \frac{-Z_A}{|\mathbf{R}_A - \mathbf{r}|} + \int \frac{\rho^X(\mathbf{r}')}{|\mathbf{r}-\mathbf{r}'|}\mathrm{d}\mathbf{r}' + \widetilde{V}^{\mathrm{X},\sigma}\right]\phi_j^{\mathrm{X},\sigma}(\mathbf{r}) = \varepsilon_j^{\mathrm{X},\sigma}\phi_j^{\mathrm{X},\sigma}(\mathbf{r}) \tag{24}$$

The effective Hamiltonian $\hat{h}^{\mathrm{X},\sigma}$ which acts on the individual MSO contains, apart from the kinetic, nuclear attraction and *Hartree* operators (the last one expressing the Coulomb repulsion with all the electrons in the system), a *corrective potential* operator, $\widetilde{V}^{\mathrm{X},\sigma}$, which differs in the two schemes (X=HF or KS), as is seen below.

A *single-determinant* N-electron function can be defined, after assigning the N electrons to the N MSOs corresponding to the lowest eigenvalues $\varepsilon_j^{\mathrm{X},\sigma}$ of equation (24), and antisymmetrizing their product:

$$\Psi_0^{\mathrm{X}} = N^{-1/2}\sum_P (-1)^{s_P}\,\widehat{P}\left[\psi_1^{\mathrm{X}}(\mathbf{x}_1)\times\cdots\times\psi_N^{\mathrm{X}}(\mathbf{x}_N)\right] \equiv ||\cdots j\cdots|| \tag{25}$$

Here $\widehat{P}$ is the general N-order permutation operator which acts on the electron coordinates and s_P the respective parity. The orthonormal MSOs which define Ψ_0^{X} are said to form the *occupied manifold*, all others belonging to the *virtual manifold*.

In the rest of this Section we shall assume, for simplicity, that we are describing a spinless system, where the occupied MSOs are in pairs having the same eigenvalue $\varepsilon_n^{\mathrm{X}}$, the same spatial part ϕ_n^{X} and α or β spin, to be labelled n^α and n^β, respectively, with $n = 1,\cdots,N/2$. In this case the spin index can be dropped from the effective Hamiltonian and from the corrective potential, since they are the same for α and β spin. Following the general definition (equations 7,9), it is easily seen that the position DM and the ED associated with $\Psi_0^{\mathrm{X}} = ||\cdots n^\alpha n^\beta\cdots||$ are simply:

$$P^X(\mathbf{r};\mathbf{r}') = 2\sum_{n=1}^{N/2}\phi_n^{\mathrm{X}}(\mathbf{r})\left(\phi_n^{\mathrm{X}}(\mathbf{r}')\right)^\star \quad ; \quad \rho^X(\mathbf{r}) = P^X(\mathbf{r};\mathbf{r}) = 2\sum_{n=1}^{N/2}|\phi_n^{\mathrm{X}}(\mathbf{r})|^2 \tag{26}$$

In the HF scheme, the corrective potential $\widetilde{V}^{\mathrm{HF}}$ is defined by imposing that the HF energy E_0^{HF} that is, the Ψ_0^{HF}-expectation value of the electrostatic Hamiltonian (which cannot be less than the true ground state energy E_0) is a minimum with respect to any other single-determinant N-electron wavefunction. Therefore, the occupied manifold resulting from the solution of equation (24) defines the optimal (in a variational sense) single-determinant approximation of the true ground state Ψ_0. To achieve this goal, $\widetilde{V}^{\mathrm{HF}}$ must take the form of the *exact-exchange operator* $\widehat{V}_{\mathrm{exch}}$, whose action on the general function $\chi(\mathbf{r})$ is defined as follows:

$$\widehat{V}_{\mathrm{exch}}\,\chi(\mathbf{r}) = -\frac{1}{2}\int\frac{P^{\mathrm{HF}}(\mathbf{r};\mathbf{r}')\chi(\mathbf{r}')}{|\mathbf{r}-\mathbf{r}'|}\mathrm{d}\mathbf{r}' \tag{27}$$

We have, correspondingly:

$$E_0^{\mathrm{HF}} \equiv \langle\, \Psi_0^{\mathrm{HF}} | \widehat{H}_{\mathrm{el}} | \Psi_0^{\mathrm{HF}} \,\rangle = -\int \left[\frac{\nabla^2}{2} P^{\mathrm{HF}}(\mathbf{r};\mathbf{r}')\right]_{(\mathbf{r}'=\mathbf{r})} \mathrm{d}\mathbf{r} - \sum_A Z_A \int \frac{\rho^{\mathrm{HF}}(\mathbf{r})}{|\mathbf{R}_A - \mathbf{r}|}\, d\mathbf{r} + \\ + \frac{1}{2}\int \frac{\rho^{\mathrm{HF}}(\mathbf{r})\rho^{\mathrm{HF}}(\mathbf{r}')}{|\mathbf{r}-\mathbf{r}'|}\, d\mathbf{r}\, d\mathbf{r}' - \frac{1}{4}\int \frac{|P^{\mathrm{HF}}(\mathbf{r};\mathbf{r}')|^2}{|\mathbf{r}-\mathbf{r}'|}\, d\mathbf{r}\, d\mathbf{r}' + \frac{1}{2}{\sum_{A,B=1}^{M}}' \frac{Z_A Z_B}{r_{AB}} \geq E_0 \tag{28}$$

The KS scheme, formulated in the frame of DFT [6, 7], introduces, for any given N-electron ED, $\rho(\mathbf{r})$, two *universal functionals*: $\varepsilon_{\mathrm{xc}}(\mathbf{r};[\rho])$ and $V_{\mathrm{xc}}(\mathbf{r};[\rho])$. The latter is obtained from the former via a functional derivative relationship: $V_{\mathrm{xc}} = \varepsilon_{\mathrm{xc}} + \rho(\delta\varepsilon_{\mathrm{xc}}/\delta\rho)$. When the *exchange-correlation potential* $V_{\mathrm{xc}}(\mathbf{r};[\rho]^{\mathrm{KS}})$ is used for $\widehat{V}^{\mathrm{KS}}$ as a multiplicative operator in equation (24), the density from equation (26) coincides with the *exact* ground-state ED (equation 11):

$$\rho^{\mathrm{KS}}(\mathbf{r}) = \rho(\mathbf{r}) \tag{29}$$

The functional $\varepsilon_{\mathrm{xc}}(\mathbf{r};[\rho])$ allows the *exact* ground-state energy to be calculated, again with reference to the occupied KS manifold:

$$E_0^{\mathrm{KS}} = -\int \left[\frac{\nabla^2}{2} P^{\mathrm{KS}}(\mathbf{r};\mathbf{r}')\right]_{(\mathbf{r}'=\mathbf{r})} \mathrm{d}\mathbf{r} - \sum_A Z_A \int \frac{\rho(\mathbf{r})}{|\mathbf{R}_A - \mathbf{r}|}\, d\mathbf{r} + \\ + \frac{1}{2}\int \frac{\rho(\mathbf{r})\rho(\mathbf{r}')}{|\mathbf{r}-\mathbf{r}'|}\, d\mathbf{r}\, d\mathbf{r}' + \int \rho(\mathbf{r})\, \varepsilon_{xc}(\mathbf{r};[\rho])\, \mathrm{d}\mathbf{r} + \frac{1}{2}{\sum_{A,B=1}^{M}}' \frac{Z_A Z_B}{r_{AB}} = E_0 \tag{30}$$

Equation (24) must be solved self-consistently in both cases, because the Hartree and the corrective potential are defi ned in terms of the occupied manifold. Two important differences between the two schemes must be stressed, however.

1. In the HF case the corrective potential (the *non-local* operator of equation 27) is perfectly defi ned. On the contrary, no exact formula exists for the *local* exchange-correlation potential $V_{\mathrm{xc}}(\mathbf{r};[\rho])$ (or equivalently, for $\varepsilon_{\mathrm{xc}}(\mathbf{r};[\rho])$) ; we shall consider in Section 3.2 some powerful though approximate expressions that have been proposed for those functionals.
2. The single-determinant wavefunction Ψ_0^{X} defi ned in equation (25) has a different meaning in the two schemes. Ψ_0^{HF} may be considered as the zero-order approximation to the true ground-state wavefunction in a hierarchy of *post-HF* methods, which re-introduce the instantaneous electron correlation (see Section 5.3). Instead, Ψ_0^{KS} is in principle only a useful mathematical construction which describes a set of non-interacting electrons in an effective potential, whose ED is the same as that of the real system. It is however customary to use Ψ_0^{KS} *as though* it were representative of some properties of Ψ_0, for instance of the off diagonal terms of the position DM $[P^{\mathrm{KS}}(\mathbf{r};\mathbf{r}') \approx P(\mathbf{r};\mathbf{r}')]$: this is what we shall do in the following. Some justifi cations for this assumption and some indications for correcting for its inadequacy have been provided, for instance, by Bauer [16].

2.2.1 HF and KS solutions: Bloch functions, insulators, metals

Some general facts about the solution of equation (24) in its spinless, periodic formulation are here recalled in order to fix notations and to prepare the discussion of the next sections.

Since the one-electron effective Hamiltonian $\hat{h}^{\mathrm{X}}$ commutes with all operations of the space group $\mathscr{S}$, in particular of the subgroup $\mathscr{T}$ of the pure translations, its eigenfunctions, the COs, can be classified according to the irreducible representations of that group. As is shown in standard textbooks [12], they are then characterized by an index κ, a vector of reciprocal space, such that the corresponding COs are *Bloch functions* (BF), $\phi_n^X(\mathbf{r};\kappa)$, which satisfy the property:

$$\phi_n^X(\mathbf{r}+\mathbf{T_m};\kappa) = \phi_n^X(\mathbf{r};\kappa)\exp(\imath\kappa\cdot\mathbf{T_m}) \tag{31}$$

Clearly, κ's differing by a reciprocal lattice vector $\mathbf{G}$ define the same irreducible representation. Among all equivalent κ's one can choose the one closest to the origin of the reciprocal space; this "minimal-length" set fills the so-called *(first) Brillouin zone* (BZ). The COs must also satisfy the BvK conditions $[\phi_n^X(\mathbf{r}+\overline{\mathbf{W}}_\mathbf{m};\kappa) = \phi_n^X(\mathbf{r};\kappa)]$, which means that $\exp(\imath\kappa\cdot\overline{\mathbf{W}}_\mathbf{m}) = 1$ or, otherwise stated, that the general κ must belong to a *Monkhorst grid* [17]:

$$\kappa_\mathbf{h} = \sum_{i=1}^{D}(h_i+s_i)\,\frac{\mathbf{B}_i}{w_i} \quad (\text{integer } h_i,\ s_i = 0 \text{ or } \frac{1}{2}) \qquad \{BvK\} \tag{32}$$

This is our standard choice: the *exact* solutions (no BvK conditions imposed) can be obtained in the limit of infinite w_i's. It is customary and useful to choose the w_i's such that the super-unit-vectors define the same Bravais lattice as the original one either "undisplaced" or "displaced" with respect to the origin according to the value of s_i. The $\kappa_\mathbf{h}$ vectors thus form a *contracted* reciprocal lattice with respect to the original one. The number of $\kappa_\mathbf{h}$ vectors in the BZ equals $W = \prod_i w_i$. As a consequence of rotational symmetry, if two sampling vectors are related to each other by a point group operator, the corresponding eigenvalues are the same, and the eigenfunctions coincide except for a rotation. This permits the determination of the solutions to be confined to $\kappa_\mathbf{h}$'s belonging to the irreducible wedge of the BZ.

As the effective number of electrons in the system is $N = WN_0$ (see Section 2), the number of occupied COs is $WN_0/2$ that is, on average, $N_0/2$ per sampling $\kappa_\mathbf{h}$ point. After ordering the eigenvalues by energy $[\varepsilon_n^X(\kappa_\mathbf{h}) \le \varepsilon_{n+1}^X(\kappa_\mathbf{h})]$, a *Fermi energy* E_F can be defined such that there are exactly $WN_0/2$ eigenvalues $\varepsilon_n^X(\kappa_\mathbf{h}) \le E_F$. A distinction can be made between insulators (including semiconductors) and metals.

With insulators, there are exactly $N_0/2$ eigenvalues below E_F at each $\kappa_\mathbf{h}$. The occupied manifold is then made of $N_0/2$ fully occupied *energy bands*. This is easily generalized to spin-polarized insulators, where the number of filled bands is different for the two spin subsystems. A unitary transformation is here feasible from the set of the occupied COs to an equivalent set of *Wannier functions* (WF) [18]:

$$\{\ldots,(n\kappa_{\mathbf{h}}),\ldots\} \overset{U}{\longleftrightarrow} \{\ldots,[\ell\mathbf{T_m}],\ldots\}$$
$$[\ell\mathbf{T_m}] \equiv w_\ell(\mathbf{r}-\mathbf{T_m}) \quad ; \quad \ell = 1, N_0/2 \quad , \quad 0 \le m_i < w_i \tag{33}$$

The WFs $[\ell\mathbf{T_m}]$ are real, localized functions which can be assigned to the general cell $\mathbf{T_m}$: due to the BvK conditions, we need to consider just W inequivalent cells e.g., those contained in the Wigner-Seitz cell of the super-lattice. There are $N_0/2$ WFs in the reference cell, all the others are translationally equivalent. Since they are obtained through a unitary transformation U from the orthonormal set of the COs, they form themselves an orthonormal set; furthermore, U can be chosen such that they are well localized according to some localization criterion, while reflecting as far as possible the rotational symmetry properties of the system [19, 20]. The ground-state wavefunction Ψ_0^X (25) for insulating spinless crystals can then be recast in the form of an antisymmetrized product of spin-WFs:

$$\Psi_0^{\mathrm{X}} \overset{\mathrm{(i)}}{=} ||\ldots[\ell\mathbf{T_m}]^\alpha[\ell\mathbf{T_m}]^\beta\ldots|| \tag{34}$$

The symbol $\overset{\mathrm{(i)}}{=}$ means that this formulation is possible only for spinless insulators.

With metals, instead, the number of eigenvalues below E_F is generally different at different $\kappa_{\mathbf{h}}$'s. Some bands are partially filled: in the limit of infinite $\mathcal{V}$'s, the surfaces in reciprocal space which separate regions with a different number of occupied COs constitute on the whole the *Fermi surface* of the metal.

2.2.2 Crystalline DM and DFs from single-determinant wave-functions

With the notations just introduced, the HF or KS DMs (equations 9, 10) can be written as follows, $\overline{f}(\mathbf{p})$ indicating the FT of $f(\mathbf{r})$:

$$P^{\mathrm{X},\sigma}(\mathbf{r};\mathbf{r}') = \sum_{\mathbf{h}}{\sum_n}' \phi_n^{\mathrm{X},\sigma}(\mathbf{r};\kappa_{\mathbf{h}})\,[\phi_n^{\mathrm{X},\sigma}(\mathbf{r}';\kappa_{\mathbf{h}})]^\star \;;\; P^{\mathrm{X}}(\mathbf{r};\mathbf{r}') = P^{\mathrm{X},\alpha}(\mathbf{r};\mathbf{r}') + P^{\mathrm{X},\beta}(\mathbf{r};\mathbf{r}')$$
$$\overline{P}^{X,\sigma}(\mathbf{p};\mathbf{p}') = \sum_{\mathbf{h}}{\sum_n}' \overline{\phi}_n^{\mathrm{X},\sigma}(\mathbf{p};\kappa_{\mathbf{h}})\,[\overline{\phi}_n^{\mathrm{X},\sigma}(\mathbf{p}';\kappa_{\mathbf{h}})]^\star \;;\; \overline{P}^{\mathrm{X}}(\mathbf{p};\mathbf{p}') = \overline{P}^{\mathrm{X},\alpha}(\mathbf{p};\mathbf{p}') + \overline{P}^{\mathrm{X},\beta}(\mathbf{p};\mathbf{p}') \tag{35}$$

where the primed sums are restricted to the occupied CSOs of σ spin $[\varepsilon_n^{\mathrm{X},\sigma}(\kappa_{\mathbf{h}}) < E_F]$, and $\overline{\phi}_n^{\mathrm{X},\sigma}$ indicates the 3-D FT of the CO. The DM expressions simplify for spinless systems:

$$P^X(\mathbf{r};\mathbf{r}') = 2\sum_{\mathbf{h}}{\sum_n}' \phi_n^X(\mathbf{r};\kappa_{\mathbf{h}})\,[\phi_n^X(\mathbf{r}';\kappa_{\mathbf{h}})]^\star \overset{\mathrm{(i)}}{=} 2\sum_{\ell,\mathbf{m}} w_\ell^X(\mathbf{r}-\mathbf{T_m})\; w_\ell^X(\mathbf{r}'-\mathbf{T_m})$$
$$\overline{P}^X(\mathbf{p};\mathbf{p}') = \frac{2}{W}\sum_{\mathbf{h}}{\sum_n}' \overline{\phi}_n^X(\mathbf{p};\kappa_{\mathbf{h}})\,[\overline{\phi}_n^X(\mathbf{p}';\kappa_{\mathbf{h}})]^\star \overset{\mathrm{(i)}}{=} 2\sum_{\ell} \overline{w}_\ell^X(\mathbf{p})\;\overline{w}_\ell^X(\mathbf{p}') \tag{36}$$

The various DFs and their properties can be obtained as discussed in Section 2.1. The following, however, should be noted.

While the KS ED, hence the corresponding structure factors, coincides in principle with the exact one (equation 29), the HF ED is expected to present systematic errors for instance, to overestimate the density in directed valence bonds (see Section 4).

HF and KS EMDs are both incorrect, but there are signifi cant differences between the two cases. Consider equations (17,18). The virial theorem is valid for HF, *not* for KS. We can therefore write, at the HF equilibrium confi guration:

$$\frac{1}{2}\int \pi^{\mathrm{HF}}(\mathbf{p})\, p^2 \,\mathrm{d}\mathbf{p} = -E_0^{\mathrm{HF}} \;<\; -E_0 \quad \left(\{\mathbf{R}\} = \{\mathbf{R}^{\mathrm{HF,eq}}\}\right) \tag{37}$$

which shows that the HF expectation value of the kinetic energy is systematically *underestimated*, but by an (approximately) known amount. The same cannot be said with the KS solution.

A notable property of the HF and KS RFF of insulators is obtained by using, in equation (19), the expression (36) of the DM in terms of WFs:

$$B^X(\mathbf{r}) \overset{\text{(i)}}{=} \frac{2}{W}\sum_{\ell,\mathbf{m}}\int w_\ell^X(\mathbf{r}'-\mathbf{T_m})\, w_\ell^X(\mathbf{r}'+\mathbf{r}-\mathbf{T_m})\,\mathrm{d}\mathbf{r}' = 2\sum_{\ell}\int w_\ell^X(\mathbf{r}')\, w_\ell^X(\mathbf{r}'+\mathbf{r})\,\mathrm{d}\mathbf{r}' \tag{38}$$

If $\mathbf{r} = \mathbf{T_n} \neq \mathbf{0}$ the last integral vanishes, since it is the overlap between WFs belonging to different cells, meaning that $B^X(\mathbf{r})$ of insulators *must be zero* at all non-zero lattice points. If such condition is not met experimentally, this could happen because of inaccuracies in the CP measurement and/or because of inadequacy of the single-determinant description of the ground-state wavefunction (see Section 4.2).

2.2.3 The problem of core electrons

A commonplace fact of chemistry is that only "valence electrons" are really involved in the formation of compounds (molecules, crystals), while "core electrons" are practically unaffected. This amounts to say that the wavefunction can be approximately written as an antisymmetrized product of $\Psi_v(\ldots,\mathbf{x}_n,\ldots)$, a wavefunction describing N_v valence electrons, times $\Psi_c(\ldots,\mathbf{x}_m,\ldots)$, which describes instead the remaining N_c core electrons; the latter can in turn be expressed as an antisymmetrized product of Ψ_c^A functions for the cores of the individual atoms A entering the compound: Ψ_c^A is obtained from the isolated atom solution except for a rigid displacement along with the nuclear coordinate. Using this core-valence separation Ansatz, which fi nds its fundamental justifi cation in the prevailing importance of the nuclear attraction term in the proximity of nuclei, the problem is formally reduced to the determination of Ψ_v^X. This can be advantageous for different reasons.

1. Since HF and KS computational times scale rather rapidly with the number of electrons (typically, as N^3), getting rid of the core electrons may result in sub-

stantial savings, especially when heavy atoms are involved where the number of valence electrons is comparatively small.
2. The all-electron wavefunction has very sharp features in the proximity of the cores. Describing them with PWs would require extremely high energy cutoffs (see for details Section 3.3.1).
3. In the vicinity of nuclei, the speed of electrons is an appreciable fraction of the speed of light, and relativistic effects become important, the more so the higher the nuclear charge; the use of the non-relativistic Hamiltonian (2) can lead to serious errors in the description of the density in that region. For instance, the relativistic correction for the form factor of the Germanium atom at κ=0.75 and 1.5 Å^{-1} amounts to about 0.6 and 1 % of the total, respectively [21]. Analytical expressions which permit the evaluation of relativistic atomic form factors up to Z=54 have been provided by Coppens and coworkers [22]. In fact, in the frame of DFT, exchange-correlation potentials $V_{\text{xc}}(\mathbf{r};[\rho]^{\text{KS}})$ have been proposed which include this kind of effects (see Section 3.2). The separation Ansatz offers an easier solution for this problem, since it allows us to use different techniques for the two terms, by limiting the relativistic treatment to the simpler (central-field) core problem for each atom.

The easiest and most popular way to exploit the separation Ansatz in the frame of HF and KS schemes is to replace in equation (24) the nuclear Coulomb potential of atom A ($-Z_A/|\mathbf{R}_A-\mathbf{r}|$) with a (generally non-local) operator $\widehat{V}_{\text{ps}}^{X,A}$, which is called the *pseudopotential* (PP) for atom A. From the solution of the modified equation, pseudo-orbitals $\psi_j^{\text{X,PP}}$ and pseudo-eigenvalues $\varepsilon_j^{\text{X,PP}}$ are obtained: the rest of the procedure is the same but only the N_v pseudo-orbitals lowest in energy are occupied.

It is not in the scopes of this Chapter to refer about the variety of PPs that have been proposed from their earliest formulations [23] to the present days. They can differ for the type of potential (local, semi-local, non-local), for the sub-division between core and valence electrons (large-core, small-core), for the criteria adopted for the optimization of the parameters involved. A number of families of PPs which cover a large part of the periodic system are included in most quantum chemical codes, and in particular in Quantum ESPRESSO and CRYSTAL.

In general, the generation of a PP for any given atom type starts from the corresponding isolated-atom solution, including relativistic corrections for its core electrons. A reference electronic configuration for the atom, typically the ground state, is chosen. The basic step in PP generation consists in replacing the "true" atomic valence orbitals with "pseudized" versions that are equal to the true ones in the outer (valence) region (i.e. for r larger than some suitable chosen *matching radius* r_c) and are smooth functions in the inner (core) region ($r \leq r_c$). In the simplest approach, the pseudized orbitals are nodeless and have the norm-conservation property, i.e. they contain the same amount of charge for $r \leq r_c$ as their atomic reference counterparts. By inverting the radial KS equation at the same eigenvalues $\varepsilon_j^{\text{KS,PP}}$ of the corresponding true valence states, $\varepsilon_{N_c+j}^{\text{KS}}$, one obtains the so-called *Norm-Conserving* PPs [24]. By relaxing the norm-conservation property of the pseudized orbitals, one obtains the *Ultrasoft* PPs (USPP) [25], having better smoothness and lesser require-

ments in terms of number of PWs. The price to pay is the presence in the charge density of *augmentation* terms to compensate for the missing charge, and the loss of a simple orthonormality relation between orbitals.

The procedure outlined above is aimed at insuring that at a distance from any core region, the PP solution resembles the all-electron one, and permits the energy for any nuclear confi guration to be obtained accurately and economically from that of the pseudo-system with reference to the energy of the constituent pseudo-atoms.

In the present context we are however interested in reconstructing DFs from the knowledge of Ψ_v^X and of the atomic core solutions. The use of PPs has a serious drawback in this respect: since the pseudo-orbitals are not orthogonal to the core, the "pseudo-charge" one gets, summed to the core density, is not the true charge density. The same is true as concerns EMD. Special techniques for all-electron charge-density reconstruction must be applied, based for example on the Projector Augmented Waves (PAW) method [26]: see Section 3.3.1.

3 The solution of the HF and KS periodic problem

3.1 General solution schemes

As shown in the previous Sections, both the HF and the KS problems can be recast under the form of single-particle Schrödinger equations under an effective self-consistent potential (Hartree and exchange potential for HF, Hartree and exchange-correlation potential for KS). The KS problem is simpler in this respect, since the effective potential depends only upon the charge density $\rho(\mathbf{r})$, while in HF it depends upon the DM $P(\mathbf{r},\mathbf{r}')$. The solution can be found using an iterative procedure to achieve self-consistency: starting from a suitable initial guess for the potential, single-particle orbitals are calculated, the effective potential is re-calculated with the new orbitals, and so on until self-consistency is achieved. Several well-established techniques for speeding up self-consistency are known. We remark however that the self-consistent solution of HF or KS equations is not the only possible way to fi nd the HF or DFT ground state. In the *global minimization* approach, one directly minimizes the energy as a function of the orbitals. This approach is perfectly equivalent to the solution of HF or KS equations. In practice, it is used only in DFT with a PW BS, for aperiodic systems or systems described by a large unit cell, and typically in conjunction with *ab-initio* molecular dynamics [27].

In practical calculations, the orbitals must be expanded into some suitably chosen BS. In periodic systems, it is convenient to use a BS of BFs $f_\mu(\mathbf{r};\kappa)$ (see Section 2.2.1), so that determining the COs $\phi_n^X(\mathbf{r};\kappa)$ reduces to a secular problem that involves only basis functions of that given κ. The choice of the BS is crucial and determines the algorithms and numerical methods used in the actual solution. Most calculations use either PWs or atom-centered functions (AOs).

PWs are the traditional choice in solid state physics, reflecting the delocalized nature of valence and conduction electron states in crystals. PWs form an infinite *complete* BS uniquely determined by the crystal lattice:

$$f_{\mathbf{G}}(\mathbf{r};\kappa) = \frac{1}{\sqrt{\Omega}} \exp[\imath(\kappa+\mathbf{G})\cdot\mathbf{r}]\,, \tag{39}$$

where Ω is the volume of the BvK box, and $\mathbf{G}$ a reciprocal lattice vector (see Section 2.1.1). The Bloch condition (equation 31) is satisfied because $\mathbf{G}\cdot\mathbf{T_m} = 2n\pi$, with integer n. A finite set can be obtained by considering all PWs whose kinetic energy, $(\kappa+\mathbf{G})^2/2$, is below a given value E_c, the so-called *kinetic energy cutoff*. PWs present several advantages:

1. They are a numerically convenient, orthonormal set, allowing the usage of Fast FT (FFT) techniques.
2. They form an *unbiased* BS, since they do not depend upon which atoms are present and upon atomic positions: therefore, they do not suffer from incomplete BS errors on forces (also known as Pulay forces [28]) or from BS superposition errors on energy (see Section 3.4.2) that affect calculations performed with AOs.
3. Convergence of the results can be evaluated by varying the single parameter E_c.

PWs have also some serious shortcomings, the most obvious being the inability to cope with the presence of core states in atoms. The standard solution is to introduce PPs, as was discussed in Section 2.2.3: in particular, USPPs [25] allow the practical usage of PWs in a large class of materials, including transition metals and first-row elements C, N, O, F. When the focus is on DFs, however, for the reasons explained there, a better solution is offered by the PAW technique, which allows the "true" all-electron charge density to be calculated, while retaining a PW BS of minimal size (see Section 3.3.1).

Even with the best USPP or PAW techology, the size of the PW BS vastly exceeds that of a well-designed basis of AOs: for typical systems, the average number of PWs per atom in the unit cell is in the order of a few hundreds. The advantages of PWs, coupled with algorithmic and numerical techniques specific for PWs, make however their usage interesting in spite of the large size of the BS, at least for DFT calculations. HF calculations in PWs are considerably slower than DFT calculations in the same system, though, and the size of the PW BS makes the expansion of the DM into PWs impractical for all but the simplest systems.

Localized BSs formed by atomic orbitals (AO), $\chi_\mu(\mathbf{r})$, are the traditional choice in quantum chemistry, reflecting the atomic composition of the matter. In periodic systems, one uses Bloch sums of AOs:

$$f_\mu(\mathbf{r};\kappa) = \frac{1}{\sqrt{W}} \sum_{\mathbf{T}} \exp[\imath\kappa\cdot\mathbf{T}]\ \chi_\mu(\mathbf{r}-\mathbf{T}) \tag{40}$$

AOs used in periodic systems include Linearized Muffin-Tin Orbitals, numerically defined Orbitals (including Slater-type orbitals) and Gaussian-type Orbitals (GTO). The CRYSTAL software described in this article shares with standard molecular

quantum chemistry codes the use of GTOs: this technical similarity entails a number of useful consequences, as analyzed in more detail in Section 3.4.2. The other main advantage of AOs is the limited number of functions required for a good description of the COs. Their main disadvantage is that they do not form a complete BS: simply adding more AOs will eventually result in pseudo-overcompleteness (i.e. linear dependencies among basis functions). As a consequence there is no mathematically exact procedure to achieve convergence with respect to the BS. Since the actual degree of convergence will depend upon the atoms that are present in the cell and upon their positions, calculations with AOs suffer from BS superposition errors on energy and have Pulay terms in forces (see again Section 3.4.2 for a more complete discussion).

In the following we describe the two approaches, PWs and AOs, with reference to the two software implementations: Quantum ESPRESSO and CRYSTAL. In both cases, however, the expression of the corrective potential $\widetilde{V}^{\mathrm{X},\sigma}$ in equation (24) must be specified, which requires (apart from the HF case) selecting one in a variety of proposals. We consider preliminarily this question by briefly examining in the next section the choices available in the two codes.

3.2 The exchange-correlation potential in KS schemes

The *quality* of the KS Hamiltonian $\hat{h}^{\mathrm{KS}}$, hence of the corresponding solution, depends primarily on the expression adopted for $V_{\mathrm{xc}}(\mathbf{r};[\rho])$, the exchange-correlation potential. Perdew [29] has suggested to classify the different proposals along a "Jacob's ladder", having at its summit the "true" potential, that is, such that equations (29) and (30) are exactly satisfied. At the lowest rung of this ladder we find the local density approximation (LDA) [7], where the exchange-correlation at $\mathbf{r}$ is a *function* of the electron density at that point: $V^{\mathrm{LDA}}(\mathbf{r}) = f^{\mathrm{LDA}}(\rho(\mathbf{r}))$. The next rung is the generalized gradient approximation (GGA) which uses also the gradient of the electron density at $\mathbf{r}$ to improve upon LDA [30]: $V^{\mathrm{GGA}}(\mathbf{r}) = f^{\mathrm{GGA}}(\rho(\mathbf{r}),\nabla\rho(\mathbf{r}))$. The third rung, denoted meta-GGA, incorporates increasingly complex ingredients, such as the kinetic energy density, $\tau(\mathbf{r})$, or the Laplacian of the density $\nabla^2\rho(\mathbf{r})$ [31]. At higher levels of the ladder non-locality in both exchange and correlation components can be included (which represents a non-standard form of the KS Hamiltonian). Hybrid-exchange functionals that use a fraction of non-local HF exchange [32] can be considered as semi-empirical fourth-rung functionals. At all levels, relativistic effects may be taken into account [33]. All these potentials contain parameters which have been variously optimized to satisfy specific requirements; for instance, Zhao and Truhlar have recently proposed modified GGA-type functionals to recover the correct gradient expansion of slowly varying densities, a quite important condition for solids [35].

Molecular and crystalline codes in current use permit one in a variety of exchange-correlation functionals to be chosen from input. Table 2 lists some that are presently available in Quantum ESPRESSO and CRYSTAL (the list is continuously enlarged,

and different combinations from those there reported can be created). Hundreds of papers have appeared where the performance of the different functionals has been tested with different families of compounds, molecules or crystals. It must be noted, however, that the basic quantity taken into account in such analyses is energy and energy derived quantities (formation energy, equilibrium geometry, vibrational frequencies...). Sometimes, other features of practical importance are considered, like the distribution of one-electron levels, etc., but almost never DFs. Suitably parameterized hybrid-exchange functionals are usually the best solution presently available in most respects: see for example reference [45]. In the following, the influence of the exchange-correlation functional on DFs is discussed by way of examples.

Type	Name	Exchange	[Ref.]	Correlation	[Ref.]	Availability	
LDA	SVWN	Slater	[36]	VWN	[37]	(E)	(C)
	SPWLSD	Slater	[36]	PWLSD	[30]	(E)	(C)
	SPZ	Slater	[36]	PZ	[34]	(E)	(C)
GGA	PBE	PBE	[38]	PBE	[38]	(E)	(C)
	PBEHCTH	PBE	[38]	HCTH	[41]	(E)	—
	PW91	PW91	[39]	PW91	[39]	(E)	(C)
	PBEsol	PBEsol	[40]	PBEsol	[40]	(E)	(C)
	SOGGA	SOGGA	[35]	PBE	[38]	—	(C)
	WC	WC	[42]	PBE	[38]	(E)	(C)
Hybrid	B3LYP	B/HF	[44]	LYP	[43]	(E)	(C)
	PBE0	PBE/HF	[38]	PBE	[38]	(E)	(C)
	B1WC	WC/HF	[42]	PW91	[39]	—	(C)

Table 2 Exchange-correlation functionals available in Quantum ESPRESSO (E) and CRYSTAL (C). Most of them are a combination of expressions for the exchange and correlation part, each described in the indicated Reference.

3.3 The Quantum ESPRESSO distribution

The Quantum ESPRESSO distribution [1] is a rather large set of packages and utilities for electronic structure calculations using DFT and a PW BS. Quantum ESPRESSO is based on a panoply of codes and tools developed and used during many years by several research groups throughout the world. It is an open-source project, currently maintained by researchers at the DEMOCRITOS National Simulation Center of the Italian National Research Council with the strong support of several other institutions and of individual researchers interested in specific subjects or in implementing new developments, as specified in the web site [1].

The package that implements the most general approach to the calculation of the ED is `PWscf`. `PWscf` can perform single-point calculations, structural optimization (including crystal cell optimization) and molecular dynamics on the electronic ground state (including variable-cell dynamics), as well as the search for transition states and minimum energy pathways. Ab-initio Car-Parrinello molecular dynamics is instead performed by package `CP`. The basic ingredient of `PWscf` is the self-consistent solution of the KS equations (24), using mixing techniques (modified Broyden) to find the self-consistent charge, and iterative diagonalization (block Davidson) to determine the COs. Iterative diagonalization does not require to store the hamiltonian H as a matrix, since only $H\psi$ products are required. Such products, as well as the ED and the Hartree and exchange-correlation potential, are calculated by taking advantage of the "dual-space technique", i.e. the possibility to jump back and forth, using the FFT algorithm, from real to reciprocal space. This allows to perform the required operations in the space where it is more convenient.

Another important package is `PHonon`, allowing the calculation of dielectric properties and of the full phonon dispersions using Density-Functional Perturbation Theory [46]. A series of tools and auxiliary codes allow the analysis of the data produced by `PWscf` and `CP`, including visualization and further processing of the ED and of the ESD.

3.3.1 The treatment of core electrons in PW codes

Let us consider the representation of the ED when simple norm-conserving PPs are used. The ED is simply given by equation (26), where the ϕ_n^{X} orbitals are replaced by the valence pseudo-orbitals $\phi_j^{\mathrm{X,PP}}$. The ED thus contains Fourier components up to a maximum value of $|\mathbf{G}|$ such that $|\mathbf{G}|^2/2 \leq E_c^\rho$, where E_c^ρ is four times larger than the kinetic energy cutoff for PWs: $E_c^\rho = 4E_c$. A three-dimensional grid in reciprocal space ("FFT grid") is introduced:

$$\overline{\rho}_{\mathrm{FFT}}(h',k',l') \equiv \overline{\rho}(\mathbf{G}_{hkl}), \quad \mathbf{G}_{hkl} = h\mathbf{B}_1 + k\mathbf{B}_2 + l\mathbf{B}_3, \tag{41}$$

where $h' = 0,\ldots,N_1-1$ and $h = h'$ if $h' \leq N_1/2$ (N_1 even) or $h' \leq (N_1-1)/2$ (N_1 odd); $h = h' - N_1$ otherwise. The equivalent relations holds for k,k',N_2 and for l,l',N_3. The values of N_1,N_2,N_3 are determined by the condition that this grid must accommodate all $\mathbf{G}$ components of ED without any loss, i.e., components for which $h = h' - N_1$ and so on should not overlap components for which $h = h'$ and so on. A three-dimensional discrete FT with dimensions N_1,N_2,N_3 then directly yields the ED on the corresponding real-space FFT grid, spanning the unit cell of the crystal:

$$\rho_{\mathrm{FFT}}(m_1,m_2,m_3) \equiv \rho(\mathbf{r}_{m_1,m_2,m_3}). \quad \mathbf{r}_{m_1,m_2,m_3} = \frac{m_1}{N_1}\mathbf{a}_1 + \frac{m_2}{N_2}\mathbf{a}_2 + \frac{m_3}{N_3}\mathbf{a}_3, \tag{42}$$

where $m_1 = 0,\ldots,N_1-1$ and the equivalent for m_2 and m_3. As mentioned earlier, the ED so obtained is actually a pseudo-density.

Let us consider now the cases of USPPs and of PAWs, which can be treated in a unifi ed framework [47]. The starting point is the introduction of a linear transformation, connecting the true orbitals ϕ_n with pseudo-orbitals ϕ_n^{PP}:

$$\phi_n(\mathbf{r}) = \mathscr{T}\phi_n^{\mathrm{PP}}(\mathbf{r}) \equiv \phi_n^{\mathrm{PP}}(\mathbf{r}) + \sum_i \left(\psi_i(\mathbf{r}) - \psi_i^{\mathrm{PP}}(\mathbf{r})\right) \langle \beta_i | \phi_n^{\mathrm{PP}} \rangle, \tag{43}$$

where the ψ_i are atomic reference orbitals (not necessarily bound states), the ψ_i^{PP} are the corresponding pseudized atomic orbitals, the β_i projectors are dual to the pseudized orbitals: $\langle \beta_i | \psi_j^{\mathrm{PP}} \rangle = \delta_{ij}$. Both $\beta_i(\mathbf{r})$ and $(\psi_i(\mathbf{r}) - \psi_i^{\mathrm{PP}}(\mathbf{r}))$ are nonzero by construction only in the core region. The sum over i runs over atoms and projectors for a given atom. Atomic functions are centered around the position of the corresponding atom.

Under suitable assumptions, one can show that the expectation value, $\sum_n \langle \phi_n | O | \phi_n \rangle$, of an operator O can be expressed as expectation value between pseudo-orbitals, $\sum_n \langle \phi_n^{\mathrm{PP}} | \widetilde{O} | \phi_n^{\mathrm{PP}} \rangle$, of an equivalent operator $\widetilde{O}$ that can be written as:

$$\widetilde{O} \equiv \mathscr{T}^\dagger O \mathscr{T} = O + \sum_{ij} |\beta_i\rangle \left(\langle \psi_i | O | \psi_j \rangle - \langle \psi_i^{\mathrm{PP}} | O | \psi_j^{\mathrm{PP}} \rangle \right) \langle \beta_j |. \tag{44}$$

With this relation, one can express the total energy as a function of smooth pseudo-orbitals $\phi_n^{\mathrm{PP}}(\mathbf{r})$, that can be easily expanded into PWs. The ED can be expressed via equation (44) by adding an "augmentation" term to the standard expression, equation (26):

$$\rho(\mathbf{r}) = 2 \sum_{n=1}^{N} \left(|\phi_n^{\mathrm{PP}}(\mathbf{r})|^2 + \sum_{ij} \langle \phi_n^{\mathrm{PP}} | \beta_i \rangle Q_{ij}(\mathbf{r}) \langle \beta_j | \phi_n^{\mathrm{PP}} \rangle \right) \tag{45}$$

The functions

$$Q_{ij}(\mathbf{r}) = (\psi_i(\mathbf{r}) \psi_j(\mathbf{r}) - \psi_i^{\mathrm{PP}}(\mathbf{r}) \psi_j^{\mathrm{PP}}(\mathbf{r})) \tag{46}$$

are nonzero only in the core region(s) of the respective atom(s). These are however quickly oscillating functions, due to orthogonality to core states, and are as such unsuitable for Fourier expansion.

Within the USPP formalism, the Q functions are in turn pseudized and transformed into equivalent but smoother functions that can be safely expanded into Fourier components. The needed cutoff, however, often exceeds the cutoff $E_c^\rho = 4E_c$ that would be needed in the absence of the augmentation term. The solution that is typically adopted for USPP is the introduction of a second FFT grid, corresponding to a cutoff $E_c^\rho > 4E_c$. The ED is thus available, both in real and in reciprocal space on this grid. The analogy with PAW suggests that the true charge density can be reconstructed by replacing the pseudized Q functions with the original, unpseudized Q functions of equation (46).

In the PAW method, instead, the augmentation term is calculated and stored on radial grids centered around atomic positions. All energy and potential terms needed in the formalism are calculated – under suitable assumptions – using either the FFT

grid or the radial grids; there are no "mixed" terms involving both grids. If the ED is desired e.g. for inspection or for visualization, however, both grids are needed.

3.3.2 The problem of "strongly correlated" systems (DFT+U)

The most commonly used DFT approximations, i.e. GGA (the "2nd rung of the ladder"), are notoriously unreliable for "strongly correlated" systems, i.e. those containing highly localized atomic-like orbitals. The big problem with DFT seems to be getting the correct occupancy of atomic-like orbitals: 3d, 4d, 5d for transition metals, 4f for rare earths, 5f for actinides, in a sea of delocalized band electrons. Current approximated exchange-correlation functionals tend to favor unphysical noninteger occupancies. Such behaviour can be traced to an important feature of the exact functional that is missing in approximate ones: a discontinuity, as a function of the number of electrons, when an integer number is crossed. This can in turn be traced to the incomplete cancellation of the self-energy, a problem that is absent by construction in HF, but is present to some extent in all approximate functionals.

DFT+U is a simple extension of conventional DFT that was devised to deal with highly correlated electrons. The basic idea of DFT+U (originally called LDA+U) is to add a Hubbard-like term for a suitably chosen subset of localized electron states [48]. The presence of (at least) an adjustable parameter U, of various possible choices for the manifold of localized states and for the Hubbard term itself, may induce to think that DFT+U is more akin to a semiempirical correction to DFT than to a real first-principle technique. Still, DFT+U is a very useful tool that has proven able to yield very good results in highly correlated materials at the price of a modest computational overhead.

Quantum ESPRESSO implements a simplified ("no-J") rotationally invariant form of the Hubbard term:

$$E_{Hub} = \frac{U}{2} \sum_{I,\sigma} \mathrm{Tr}\left[\mathbf{n}^{I\sigma}(1 - \mathbf{n}^{I\sigma})\right] \tag{47}$$

where $\mathbf{n}^{I\sigma}$ is the occupation matrix on the chosen manifold of localized states for atom I, for spin σ, and U is the Hubbard parameter [49]. The occupation matrix is defined as

$$n^{I\sigma}_{mm'} = \sum_n f^{\sigma}_n \langle \phi^{\sigma}_n | P^I_{mm'} | \phi^{\sigma}_n \rangle \tag{48}$$

where $P^I_{mm'}$ is the projector over the chosen manifold of localized states, f^{σ}_n the occupation (between 0 and 1) for electron orbital ϕ^{σ}_n. Typically the projector P simply projects over atomic states, and only on strongly localized ones (e.g. 3d in first-row transition metals and so on). The most delicate decision in a DFT+U calculation is probably the choice of the parameter U. For each atom in a given electronic configuration, experience and experiments indicate a typical range for U, usually a few eV. One can use U as an adjustable parameter; a more satisfactory procedure, described in Reference [49], allows a consistent value of U to be determined from

first principles. The introduction of the U parameter may have profound effects on the electronic structure, and as a consequence, on the charge density of strongly correlated materials.

3.4 The CRYSTAL package

3.4.1 General features

CRYSTAL was conceived more than thirty years ago [50] as an extension to periodic systems of the powerful ab-initio molecular codes which were available at that time [51, 52, 53]. It has since been developed by researchers of the Theoretical Chemistry Group in Torino (Italy) and of the Computational Materials Science Group in Daresbury (UK), with important contributions from other scientists, as documented in the CRYSTAL site [2]. CRYSTAL solves the periodic HF and KS equations with a variety of exchange-correlation potentials (see Table 2). As in the molecular codes that served as its template, it adopts a BS of GTOs; this choice has some advantages and drawbacks as already anticipated in Section 3.1, and as analyzed in more detail in Section 3.4.2. An attractive feature related to the *local* character of the basis functions is that not only 3-dimensional crystals, but also structures periodic in 2 (slabs), 1 (polymers) and 0 (molecules) dimensions are treated by CRYSTAL with the same basic technology without any need of artificial replication of the subunits. In all cases, the symmetry of the system is fully exploited: for instance in carbon nanotubes (a 1-dimensional polymer), profit can be taken of the helicoidal symmetry with substantial time savings [54]. Among the many facilities embodied in CRYSTAL we list below some which are of interest in the present context.

1. Full geometry optimization is feasible with respect to both lattice parameters and atomic positions. It is also possible to perform *volume constrained* geometry optimization: that is, for a given crystalline structure and for a given cell volume V, the minimum energy configuration is determined. From the corresponding $E(V)$ curves, the effect of pressure on various properties of the system, including DFs, can be determined.
2. The vibrational frequencies at $\kappa = 0$ (Γ) and the corresponding infrared intensities are determined in the harmonic approximation; an anharmonic correction is performed for the stretching mode of X-H bonds. Each normal mode is classified by symmetry and can be visualized. The comparison with experimental vibrational data becomes easy, and often results in extremely good agreement [55]. Zero-point-motion and finite-temperature effects can be determined in the frame of the harmonic approximation (there may be the need of complementing the information at Γ with that at other points in the BZ, which may be obtained from supercell calculations). The knowledge of nuclear motions can be used for estimating Debye-Waller atomic factors or, more generally, for obtaining an ensemble description of electronic DFs at finite temperatures (see Section 5.1).

3. All-electron calculations are feasible in all cases, and are preferable to PP ones when one is interested in DFs for the reasons discussed in Section 2.2.3. Note however that no relativistic corrections for core electrons are yet implemented in CRYSTAL.
4. Various tools are available for representing the ED and calculating the static structure factors. Among the examples provided below of the use of these tools, one concerns the "ED deformation map" of a molecular crystal, that is, the difference between the density in the actual system, and the superposition of the densities of the isolated molecules at the geometry they have in the crystal (see Section 4.2).
5. An essential descriptor of EDs is Bader's topological analysis (see Section 2.1.1). CRYSTAL is connected to Gatti's TOPOND program [56] in the sense that it provides the latter with the information required for determining all topological properties of interest (see Chapter 1 in this Book).
6. The EMD, the directional CPs, the reciprocal form factor $[B(\mathbf{r})]$, and their anisotropies can be calculated in different ways which provide results of different accuracy according to the nature of the system (insulator, conductor). Again, examples are provided below.
7. The effect of a static, uniform external electric field on the DM can be studied in CRYSTAL in two ways, either by superimposing a sawtooth potential (which preserves periodicity on a supercell scale), or by calculating the first and second derivatives of the DM with respect to the field components in the frame of coupled-perturbative HF or DFT: see Section 5.2 for more details.
8. In its most recent version CRYSTAL is connected to CRYSCOR, a post-HF code which permits the correction to the energy and to the DM of the crystalline system to be calculated at the lowest order of perturbation theory (see Section 5.3).

3.4.2 The basis set problem

CRYSTAL shares with standard molecular codes the use of GTOs as basis functions. Each atom A carries p_A GTOs, each resulting from a "contraction" of M_{iA} Gaussian "primitives" of angular momentum components ℓ, m centered in $\mathbf{R}_A$:

$$\chi_{iA}(\mathbf{r}_A) = \sum_{j=1}^{M_{iA}} c_{iA,j}\, N^{\ell,m}(\alpha_{iA,j})\, X^{\ell,m}(\mathbf{r}_A)\, \exp[-\alpha_{iA,j}\, \mathbf{r}_A^2]\,.$$

Here $\mathbf{r}_A = \mathbf{r} - \mathbf{R}_A$, $X^{\ell,m}$ are real solid harmonics and $N^{\ell,m}$ normalization coefficients; $c_{iA,j}$ are known as "coefficients", $\alpha_{iA,j}$ as "exponents" of the GTO. As a rule, $\mathbf{R}_A$ are nuclear coordinates, but GTOs on "ghost atoms" at a general position can be added.

From its beginnings, CRYSTAL took over from molecular quantum chemistry the experience gained in the preparation of these sets and the extremely efficient algorithms already available for performing one- and two-electron GTO-integrals. During all these years other innovations were imported from computational quantum chemistry, related to the use of GTOs. Just to mention an example, density-

fi tting techniques, which permit incredible savings of time in the calculation of the integrals needed in post-HF schemes [57], can be transferred with few modifi cations to periodic GTO-based schemes (see Section 5.3). Another side advantage of the sharing of the same BS, is the possibility of one-to-one comparisons between the results of periodic and standard molecular calculations; examples thereof are provided below.

The evaluation of GTO-integrals in CRYSTAL entails problems related to the periodically infi nite character of the system. Sophisticated techniques have been implemented which permit the truncation or the accurate approximation of lattice sums: Ewald techniques, multipolar treatment of non-overlapping distributions, bipolar expansion, etc. On the whole, many thousand lines of code have been developed for this purpose, which contrasts the amazing simplicity of the corresponding integral part in PW codes.

The real problem with GTO sets, however, is their inherent incompleteness. For each system, for each atomic species inside, a choice must be performed of the number (p_A), type (ℓ, m) and contraction scheme (M_{iA}, $c_{iA,j}$, $\alpha_{iA,j}$) of the χ_{iA} functions. Again, this contrasts with PW sets which are complete, in principle, and whose quality is determined by a single parameter (the energy cutoff). An enormous literature exists on how to set up GTO sets which perform effi ciently for different types of system. The quality of the GTO set on atom A can in principle be improved at will by including more and more χ_{iA} functions, for instance following a precise strategy [58]. Techniques for extrapolating the computed energy to the *complete BS limit* have also been proposed [59]. For atoms in crystals, a number of AE or valence-only GTO sets are proposed in the CRYSTAL site, based on past experience [2]; those suggested for oxygen, for example, are different according to whether this species is present as an oxide ion (as in MgO) or is involved in semi-covalent bonds (Ice). A clever choice permits a very accurate representation of the ground state (HF, KS) wavefunction to be obtained with a surprisingly small number of functions, as compared to PWs.

Two additional problems can fi nally be mentioned.

1. The potential energy surface, $E_0(\{\mathbf{R}\})$, that is, the dependence of the calculated ground-state energy on the set of the nuclear coordinates, bears crucial importance because it determines not only reaction energies, but also equilibrium confi guration and vibrational frequencies which directly influence DFs. In order to have reliable values for these quantities, all errors that affect $E_0(\{\mathbf{R}\})$ should be approximately constant over the range of nuclear coordinates considered. The part of this error related to the dependence of BS quality on $\{\mathbf{R}\}$ is known as BSSE (BS superposition error) [60]. It affects in particular schemes, such as CRYSTAL, using GTO functions centered in the nuclei: it is generally expected that the same GTO set describes better structures where atoms are close to each other than viceversa because in the former case the wavefunction in the interatomic regions can be represented more accurately using "redundant" functions from neighboring atoms. Many techniques have been proposed to estimate the BSSE and to correct for it [61]. The automated geometry optimization in CRYS-

TAL, however, does not take BSSE into account, and may therefore result into too compact structures, for the reasons just explained.

2. The use of extended atomic sets comprising very diffuse (low exponent) primitives may lead to quasi-linear-dependence effects between functions centered in different atoms. With densely packed systems as are encountered in solid state problems, this type of "overcompleteness" easily results in catastrophic behaviour. As concerns the use of high angular momentum functions, the present version of CRYSTAL is limited to $\ell \leq 3$ (s, p, d, f GTOs).

4 Role of computational parameters on density functions

We provide below a few examples of simulated DFs for crystalline systems obtained with the two programs described in the previous Section. Different computational choices and their consequences on the results will be considered in the various cases. The objective is to provide an outlook of present capabilities and an indication of possible pitfalls due to unwise selection of the computational parameters. The cases of two typical covalent systems (Silicon, Diamond), of a molecular crystal (Urea) and of a metal (Aluminium) are considered. As concerns ionic systems (LiN_3, MgO, for instance), reference can be made to the existing literature [62, 63]. Finally, the effect of the Hamiltonian on spin localization in an ionic spin-polarized system ($KMnF_3$) is discussed.

4.1 ED of Silicon and Diamond: Basis set and Hamiltonian effects

Silicon and Diamond are two prototypical covalent systems: for this reason and for their intrinsic importance, they have been devoted enormous attention to. Among the many papers concerning the properties of their DM (see for instance the recent synchrotron-radiation experiment with powder samples [64]), we will refer in the following to the study by Lu *et al.* [21], who compared the EDs resulting from their all-electron LDA calculations for Diamond, Silicon and Germanium with those from experimental data, and in particular from accurately analyzed X-ray diffraction data for crystalline Silicon. Reference can also be made to the comprehensive studies performed with CRYSTAL about contemporarily [65, 66], and aimed at analyzing the quality of quasi-HF periodic solutions for this kind of systems. Here we consider the effect on the calculated ED of the quality of the representative BS and of the type of Hamiltonian adopted, by taking advantage of the availability of the two computational tools. Silicon is first considered in more detail; similar results are next reported for Diamond.

Figure 1 documents the BS dependence of two quantities related to the ED: its value at the Si-Si midpoint (δ) and the "forbidden" F_{222} structure factor, whose non-zero value is a measure of the asphericity of the ED about the individual

atoms (see Section 2.1.1). All data here shown were obtained with the PBE choice for $V_{xc}(\mathbf{r};[\rho])$ (see Section 3.2), but very similar trends were obtained with other choices; the lattice parameter was set at its experimental value, a = 5.43 Å. The Quantum ESPRESSO calculations were performed using the PAW technique (see Section 3.3.1; PAW pseudopotentials were generated using the parameters given in `paw_library`, contained in the Quantum ESPRESSO distribution). Different E_c values were tried as shown in the figure; correspondingly, the cutoff for the core contribution was varied from 48 to 120 Ry. As concerns the sampling in **k** space, a displaced Monkhorst grid with w=4, s=1/2 for all i's (see equation 32) was generally adopted, which may be labelled K4'; the adequacy of this choice is demonstrated in the left panel, which shows the effect of using different undisplaced (Kw) or displaced (Kw') k-grids with E_c=20 Ry. In the CRYSTAL all-electron calculations, a K8 sampling net was used, and a number of GTO sets were tried, which can be classified in two categories. The former category comprises double-zeta 8-41G sets as in reference [66], complemented with n (the number of asterisks) polarization functions of type d, d+d, d+d+f, respectively; the 8-41G***(sp) includes in addition a single-GTO sp set at the midpoint of each bond, with exponent 1.4 a.u. The latter category comprises the 6-21G and 6-21G* sets as in reference [66].

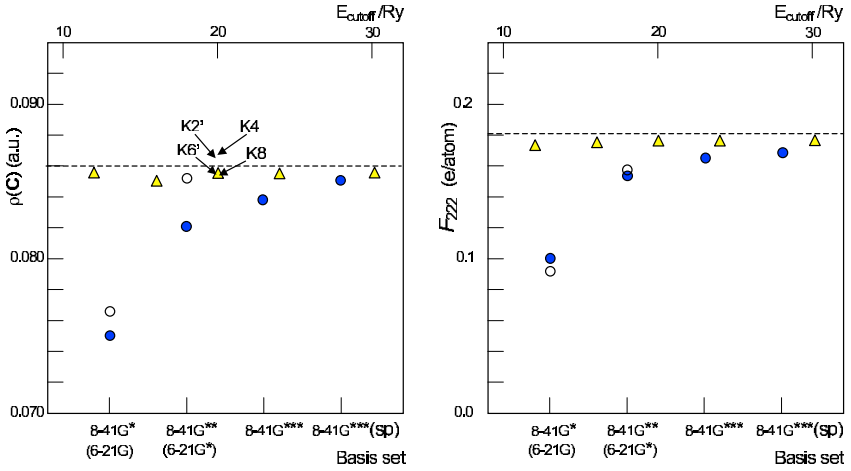

Fig. 1 Effect of basis set quality on $\rho(\delta)$, the calculated ED at the bond midpoint (left panel) and on the F_{222} structure factor (right panel) for crystalline Silicon, using the DFT-PBE Hamiltonian. The Quantum ESPRESSO results (triangles) are reported as a function of the cutoff energy E_c (scale on top); the CRYSTAL ones along an arbitrary scale (at bottom) corresponding to GTO sets of increasing quality: 8-41G^{n*} (full circles) or 6-21G^{n*} open circles). The two horizontal dashed lines indicate the estimated experimental value [21]. See text for other details.

The regular trend of the Quantum ESPRESSO results is clear and, as far as these quantities are concerned, the limit with respect to E_c seems reached. The CRYSTAL results are more scattered, as expected. Note in particular that the 6-21G* results are curiously very similar to the best PW results, which represents a warning against too hasty conclusions about the adequacy of the adopted BS. From the present data it

appears in fact that convergence of the GTO sets towards the BS limit may be slower for DM related quantities than for energy: the PBE energy per cell for the three best GTO sets here used is -578.7798, -578.7821, -578.7826 E_h, respectively.

The converged results are also quite close to the data proposed by Lu *et al.* [21], by extrapolation to zero thermal motion of the best experimental results: $\rho(\delta)$ = 0.086 a.u., F_{222} = 0.181 e/atom.

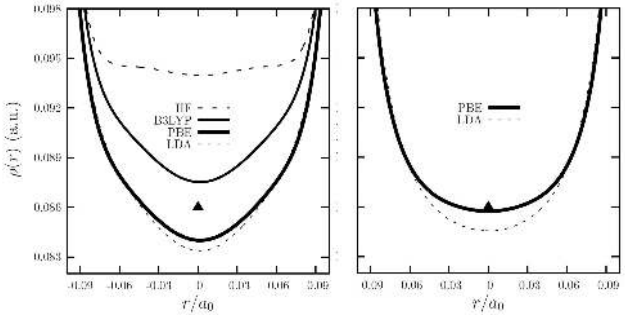

Fig. 2 Silicon ED along the Si-Si bond with different one-electron Hamiltonians, as indicated, and using either CRYSTAL (left panel) or Quantum ESPRESSO (right panel). The triangles are the experimental value [21].

Figure 2 reports the ED along the Si—Si bond for various Hamiltonians (see Section 3.2), as a function of the distance r from the bond midpoint in units of the lattice parameter. For the CRYSTAL calculations (left panel), the 8-41G***(sp) GTO set was used. For the Quantum ESPRESSO calculations (right panel), a K4' grid and a cutoff of 30 Ry were adopted; the core charge and the augmentation term in the valence charge were directly plotted in real space. Note that in the present version of this code, the PAW technique cannot be used with non-local exchange Hamiltonians. The LDA functionals SVWN and PZ have been used with the two codes, respectively. According to the CRYSTAL calculations, close to the bond midpoint the HF EC lies highest followed by the hybrid functional (B3LYP), the GGA (PBE), and the LDA ones; the Quantum ESPRESSO results with the pure DFT Hamiltonians are almost the same.

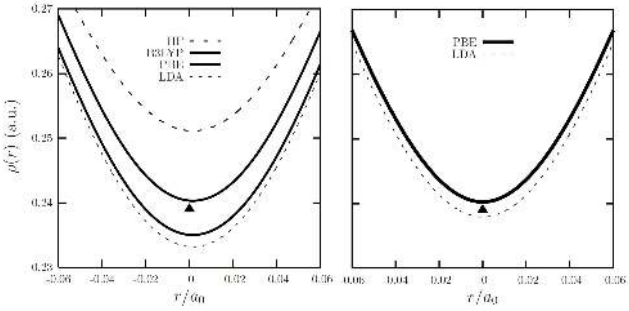

Fig. 3 Diamond ED. Symbols as in Figure 2.

Results similar to those just presented were obtained with Diamond (see Figure 4.1). Again, the experimental geometry was adopted (a = 3.567 Å); a 6-31G** GTO set taken from the literature [65] complemented with an additional f-type polarization set was used for the CRYSTAL calculations (left panel); for the Quantum ESPRESSO ones (right panel), a K4' grid and a cutoff of 45 Ry were adopted.

For the two systems, the ED presents a Bader critical point of type (3,+1) at the bond midpoint δ, and its value increases steadily moving away from it along the bond. The case is different if one considers only the contribution to the ED from valence electrons, $\rho_{\rm val}(\mathbf{r})$. An "experimental" determination of this non-observable quantity can be obtained by subtracting from the reconstructed ED the contribution of core electrons from accurate atomic calculations: both in silicon and in diamond $\rho_{\rm val}$ presents a relative maximum at two symmetry related points (γ) when moving from δ towards the cores [21]: in the case of silicon the difference between the two values is almost undetectable experimentally. It may be interesting to compare these experimental data with those from CRYSTAL all-electron calculations (but using only the valence bands in the primed sums of equation 35), or from Quantum ESPRESSO valence-only computations because the differences between the various schemes become so more evident (see Table 3). The computational conditions are as before; in particular, with CRYSTAL, two GTO sets of comparable quality: 8-41G*** and 6-31G**, have been used for silicon and diamond, respectively; in the PW calculations, norm-conserving pseudopotentials from the Quantum ESPRESSO library [1], a K4' grid and cutoffs of 30 and 70 Ry for Silicon and Diamond, respectively, were adopted. The agreement with the experimental determinations is generally excellent, the hybrid B3LYP functional performing particularly well. The HF data appear to exaggerate the value of $\rho(\delta)$ for both systems.

		Silicon			Diamond		
Hamiltonian	BS	$\rho_{\rm val}(\delta)$	$\rho_{\rm val}(\gamma)$	$\Delta\rho_{\rm val}$	$\rho_{\rm val}(\delta)$	$\rho_{\rm val}(\gamma)$	$\Delta\rho_{\rm val}$
HF	GTO	0.093	0.094	0.001	0.251	0.285	0.034
	PW	0.095	0.095	0.001	0.261	0.300	0.039
B3LYP	GTO	0.087	0.088	0.001	0.240	0.285	0.045
	PW	0.089	0.091	0.002	0.247	0.307	0.060
PBE	GTO	0.084	0.085	0.001	0.235	0.281	0.044
	PW	0.085	0.086	0.001	0.240	0.300	0.061
LDA	GTO	0.083	0.084	0.001	0.233	0.280	0.047
	PW	0.084	0.086	0.002	0.242	0.295	0.053
Experiment [21]		0.086	0.086	0.000	0.240	0.287	0.048

Table 3 Valence electron density data (a.u.) for silicon and diamond at the experimental geometry: δ is the bond midpoint, γ the location of the maximum along the bond; $\Delta\rho_{\rm val} = \rho_{\rm val}(\gamma) - \rho_{\rm val}(\delta)$ the depth of the minimum. See text for the computational conditions and other details.

4.2 Environmental effects on the DFs of a molecular crystal: Urea

In a molecular crystal the constituent molecules are clearly identifiable even if in a geometry slightly different from the one they have in the gas phase. In the case of urea, the one treated in this Section, there are two symmetry-equivalent molecules per unit cell whose bond lengths and angles are modified to a small extent with re-

[1] For Si: `Si.pbe-rrkj.UPF`, `Si.pz-vbc.UPF`, `Si.blyp-rrkj.UPF`; for C: `C.pbe-mt.UPF`, `C.pz-vbc.UPF`, `C.blyp-mt.UPF`.

spect to the free molecule (in particular, they take a planar confi guration). On the whole, however, the weak interactions which set in between the molecules when the crystal is formed do not alter in any essential way their electronic structure. In order to make evident the role of intermolecular forces on DFs, it is then customary to consider so-called *interaction* DFs, $\Delta\rho(\mathbf{r})$ and $\Delta\pi(\mathbf{p})$. Reference is made for this purpose to a *procrystal* formed by $\overline{N}$ molecules in the unit cell (two in our case) and from all their translationally equivalent copies, in the same geometry and position they have in the crystal, but mutually independent. For each of those pseudomolecules ($M = 1,\overline{N}$), the appropriate DF $[\rho^M(\mathbf{r}),\ \pi^M(\mathbf{p})]$, is computed using the same technique as for the crystal $[\rho^{\mathrm{cry}}(\mathbf{r}),\ \pi^{\mathrm{cry}}(\mathbf{p})]$. We can so defi ne:

$$\Delta\rho(\mathbf{r}) = \rho^{\mathrm{cry}}(\mathbf{r}) - \sum_{M,\mathbf{T}} \rho^M(\mathbf{r}-\mathbf{T}) \quad ; \quad \Delta\pi(\mathbf{p}) = \pi^{\mathrm{cry}}(\mathbf{p}) - \sum_{M} \pi^M(\mathbf{p}) \quad (49)$$

In the second equation, we have exploited the independence of FTs from the origin, and used the normalization convention of Section 2.1.

The effect of the crystalline environment on the DFs of urea has been the object of intense experimental and theoretical work, because of the simple and at the same time intriguing structure of this system. In the crystal, the urea molecules are arranged top-to-tail to form two series of planar tapes, oppositely oriented and mutually orthogonal; hydrogen bonds are the main responsible for the links within the tape and between the tapes: the terminal oxygen of each molecule is thus forming four such bonds, an almost unique feature in molecular crystals.

Probably the most complete study to date of the ED of crystalline urea is the one by Birkedal *et al.* [67], who have reported synchrotron diffraction data of unprecedented precision, very accurately analyzed; the reconstructed experimental ED is there compared to that resulting from periodic HF calculations, by considering the respective characterization of the most important critical points owing to Bader's theory [8]. Gatti has recently reviewed the power of this theory using precisely urea as a test case [10] and extending the analysis performed in a pioneering ab-initio HF study [68]: in particular, he demonstrated the ability of topological analysis to describe quantitatively environmental effects on the ED, both as concerns the intermolecular and, indirectly, the intramolecular region (for instance, the appreciable change of the dipole moment of the molecule in the crystal with respect to its gas-phase value). The important discussion about the detectability of environmental effects from diffraction data by Spackman *et al.* [69] is also worth mentioning.

While in those studies only one type of periodic computation was considered (HF, with GTO BSs of rather good quality), we document here briefly the influence of Hamiltonian and BS on the description of $\rho(\mathbf{r})$ and $\Delta\rho(\mathbf{r})$, and extend the discussion to EMDs; for the latter case, which has been the object of a recent study by some of us [70], only results obtained with CRYSTAL are reported, because the analysis of EMDs is not yet feasible with the current version of Quantum ESPRESSO. In the following, all calculated data are referred to the experimental crystalline geometry [71] in order to make them comparable to each other and to the experimental data. Some of the GTO sets here used are taken from recent theoretical studies performed with CRYSTAL on urea and other molecular crystals [72, 73]; in

order of increasing quality: 6-31G(d,p) [here and in the following, the first set of polarization functions is assigned to first row atoms C,N,O, the second to H]; 6-311G(d,p); 6-311G(2df,2pd); TZPP; QZVPP. The last two GTO sets belong to a family devised by Ahlrichs and coworkers [74].

Figure 4 reports total and interaction ED maps obtained from HF CRYSTAL calculations with a very good (TZPP) GTO set. The picture is very similar to that provided by Spackman *et al.* [69]: with respect to the superposition of molecular densities the most notable feature is a build-up of charge in front of the terminal oxygen, due to the population of the hydrogen bonds with the neighboring molecule and to the corresponding de-population of the N-H intramolecular bonds.

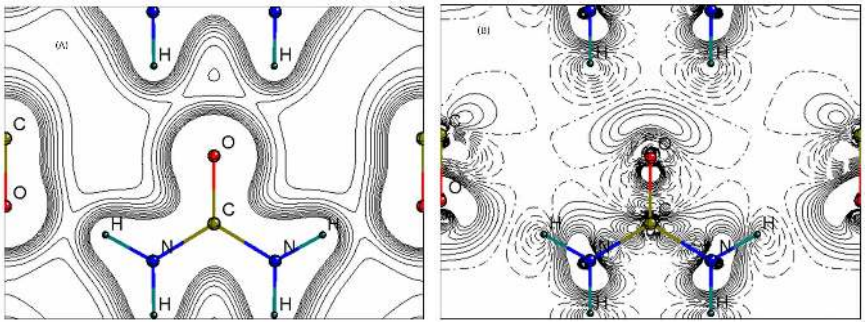

Fig. 4 Total (left panel) and interaction (right panel) charge density of crystalline urea in the (110) plane, resulting from HF calculations using a TZPP GTO set (see text). In the $\rho(\mathbf{r})$ map, the distance between consecutive lines is 0.01 a.u.; in the $\Delta\rho(\mathbf{r})$ map, it is 0.001 a.u.

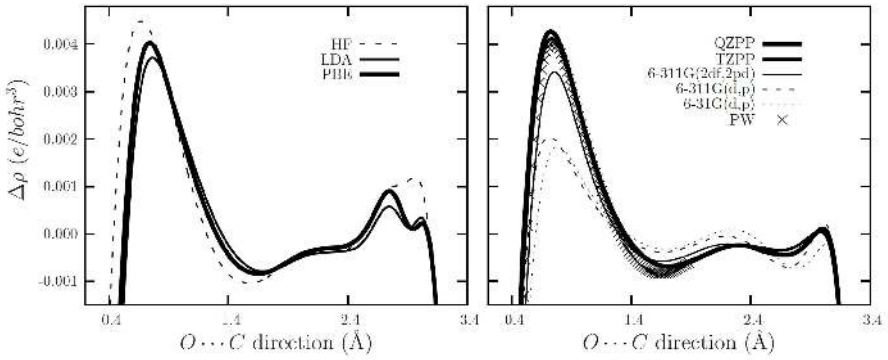

Fig. 5 Charge interaction density $[\Delta\rho(r)]$ along the $O\cdots C$ intermolecular direction (origin at O). The plots on the left, obtained with Quantum ESPRESSO, show the dependence on the Hamiltonian. Those on the right, the dependence on the BS for the PBE Hamiltonian: they were obtained with CRYSTAL except for the PW result, taken from the left panel. See text for details.

Figure 5 describes the interaction ED along the line from the terminal O to the central C in the neighboring molecule, at a distance of 3.42 Å: this may not be the direction where environmental effects are the largest [10], but allows both inter- and intra-molecular changes of the ED to be recorded. The left panel shows the dependence on the Hamiltonian, as resulting from Quantum ESPRESSO calculations. In fact, in this case the procrystal was simulated by only two molecules, those containing the two selected atoms: therefore, $\Delta\rho(r)$ is not accurate beyond 2.4 Å from O, where the densities of other molecules become comparatively important. A cutoff E_c=50 Ry was used, practically corresponding to convergence: the HF and LDA solutions represent again two extremes as concerns the entity of the interaction density. The right panel, which refers to PBE calculations with different BSs, performed with CRYSTAL and using the complete procrystal, shows that convergence towards the PW solution in a vicinity of the O atom is achieved only with very sophisticated GTO sets. Interestingly, convergence of the calculated cohesive energy of the crystal to within 1 kJ/mol could be reached even when considering GTO sets of 6-311G(2df,2pd) quality [72, 73]: this shows again that DFs can be more sensitive to BS quality than energy related quantities.

The question has been raised by Spackman *et al.* [69] whether these environmental effects, unambiguously revealed by theoretical investigations, can be detected from experimental structure factors. In spite of the availability of new high quality data obtained either via X-ray [75] or synchrotron diffraction [67] and of very sophisticated tools for their interpretation, the debate on this matter is still open.

Information from directional CPs is shown below to provide clearer evidence of the effect of the crystalline environment on the DM of urea; also the level adopted for its theoretical description appears to play here a more relevant role.

We have considered the CPs in the main three crystallographic directions: [001], along the tapes and perpendicular to the other two; [100], forming an angle of $\pi/4$ with the planes containing the tapes; [110], parallel to one set of tapes and perpendicular to the other. The experimental CP *anisotropies* $[J_{hkl}(p) - J_{h'k'l'}(p)]$, obtained from very accurate measurements using synchrotron radiation [76], can be compared directly with the calculated ones after correcting the latter for the limited experimental resolution (see Section 2.1.2). In examining the influence of the Hamiltonian on EMDs, we have also performed post-HF MP2 calculations, owing to the scheme (*b*) described in Section 5.3. We don't analyze here the important effects of BS quality, and report only the results obtained with the best BS feasible with all techniques, namely the 6-311G(d,p) BS previously introduced.

Two independent CP anisotropies, $[J_{001}(p) - J_{100}(p)]$ and $[J_{110}(p) - J_{100}(p)]$, are shown in Figure 6. The first one is comparatively large, since it describes in a way the difference between the EMD in the direction of the tapes and perpendicular to them; the second one, between the two perpendicular directions, is much smaller, as expected, and still reveals the extreme sensitivity of CPs to directional effects. Comparison of the CP anisotropies for the crystal and the procrystal, the latter obtained following the scheme of equation 49, shows that environmental effects are clearly visible, both from the experimental and the theoretical viewpoint. Inspection of the

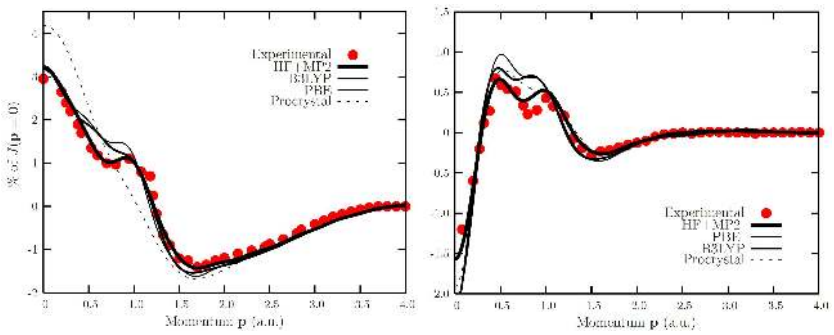

Fig. 6 CP anisotropies of urea: $[J_{001}(p) - J_{100}(p)]$ (left panel) and $[J_{110}(p) - J_{100}(p)]$ (right panel), obtained with different techniques (see inset), and given as percentage of the respective $J_{001}(0)$ value. All theoretical data were corrected for the experimental resolution.

results obtained with the different Hamiltonians, indicates that the HF+MP2 approach gives defi nitely better results than DFT, especially at intermediate moments. This is not unexpected (see Section 2.2): the MP2 method, taking advantage of the exact description of the electronic Fermi (exchange) correlation already provided by the reference HF method, can also recover a signifi cant portion of the dynamic Coulomb correlation of the electronic motions. On the contrary, DFT describes both Fermi and Coulomb correlation as an average on the ground-state charge density and therefore cannot perform particularly well in predicting EMDs [77, 78].

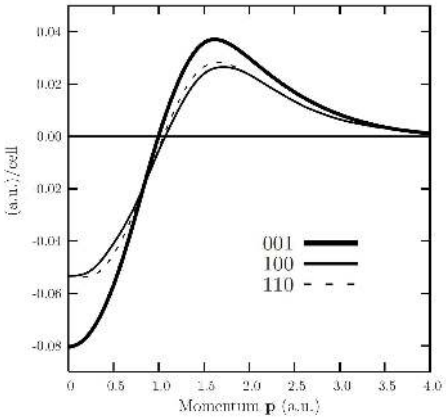

Fig. 7 Correlation contribution $J_{hkl}^{\mathrm{MP2}}(p)$ to the three CPs along the main crystallographic directions [001], [100], and [110].

Figure 7 shows $J_{hkl}^{\mathrm{MP2}}(p)$, representing the correlation correction to the HF CP, $J_{hkl}^{\mathrm{HF}}(p)$, in the three directions. This correction is small (well within 1% of $J_{001}(0)$, whose value is $\approx$24.70 a.u.) and would be hardly visible in the scale of Figure 6. Two features can be noted, however: i), the MP2 correction is negative at low momenta,

positive at high momenta, corresponding to the higher average kinetic energy of correlated electrons and, ii), this correction reduces the HF CP anisotropies.

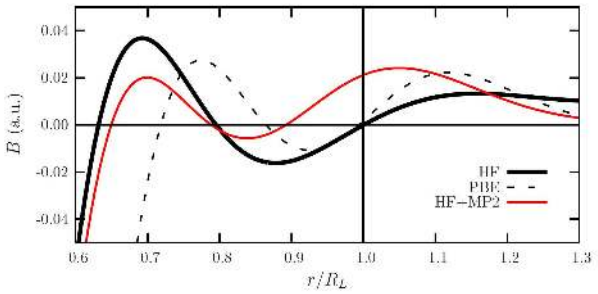

Fig. 8 Directional RFF $B_{001}(r/R_L)$ calculated with different techniques, as indicated. R_L=8.84 a.u. is the length of the first non-zero lattice vector along the [001] direction.

More direct evidence of correlation effects is provided by the directional RFFs (see Sections 2.1.2 and 2.2.3). Consider the data of Figure 8. The RFFs along the [001] direction calculated with different Hamiltonians are there reported at an intermediate range as a function of the ratio r/R_L, R_L being the length of the first non-zero lattice vector in that direction. Equation 38 tells us that all RFFs obtained from single-determinant wavefunctions must be zero at r/R_L=1, independently of the BS used. This is in fact what is observed in the two examples reported (HF, PBE), and the same has been verified to happen in all cases and for all directions, provided that the calculations are numerically accurate. It is noteworthy that the MP2 correction, though minute, results in a significant departure from such zero condition. This indication is susceptible of an easy experimental check, which is however not possible from the data provided in reference [76].

4.3 ED, EMD, CPF of simple metals: the case of Aluminium

The accurate determination of the DM of metals involves a number of special problems, both fundamental and technical, which can be schematically stated as follows with reference to the prototypical metallic system, namely the *electron gas* [79].

1. The single-determinant description of this system is by necessity an antisymmetrized product of PWs: $\phi_n^X(\mathbf{r};\kappa) \propto \exp(\imath\kappa\cdot\mathbf{r})$ or $\phi_n^X(\mathbf{p};\kappa) \propto \delta(\mathbf{p}-\kappa)$. Since the associated eigenvalue $\varepsilon_n^X(\kappa)$ monotonously increases with $|\kappa|$ (in a way depending on X), the occupied ground-state manifold fills a sphere in reciprocal space centered in the origin and of radius $K_F = (3\rho/8\pi)^{1/3}$, where $\rho = N/V$ is the number of electrons per unit volume. As is clear from equation (36), the corresponding EMD has then the constant value $2/\rho$ for $|\mathbf{p}| < K_F$, zero otherwise. For real metallic systems, these features are obviously modified but the change in the number of occupied states at the two sides of the Fermi surface always results in a sharp discontinuity in the EMD at $\mathbf{p} = \kappa_F + \mathbf{G}$ where κ_F lies on the Fermi surface and $\mathbf{G}$ is a reciprocal lattice vector. This is an intrinsic deficiency of one-

electron approximations. A many-body analysis of the interacting-electron-gas problem shows in fact that, due to electron correlation, the discontinuity of the EMD at K_F exists indeed, but is not as sharp: $\pi(\mathbf{p})$ has a non-zero tail also for $|\mathbf{p}| > K_F$, compensated for by a decrease of the EMD for $|\mathbf{p}|$ below K_F. Explicit expressions for correcting EMDs from one-electron approximations have been proposed by Lundqvist and Lydén [80] and by Lam and Platzman [81].

2. The HF description of the DM of the free electron gas coincides with that provided by any one-electron Hamiltonian. This is no longer true when real metals are considered, in particular as concerns the ED, for which the KS equation gives in principle the exact result. One may wonder how the two kinds of approximation perform when considering the EMD of metals. For this kind of systems HF is usually mistrusted because the κ dependence of the HF free-electron eigenvalues, $\varepsilon_n^{HF}(\kappa)$ has an unphysical logarithmic singularity at $|\kappa| = K_F$. While this fact has unpleasant consequences on band structures, it hardly influences DFs, as is shown below.
3. From a technical viewpoint, it is generally believed that GTF BSs (or any set of atom-centered local functions) cannot adequately describe conduction electrons, and that the use of PWs is nearly mandatory.

The case of Aluminium is here briefly considered in order to provide indications on the influence of these problems on calculated DFs of metals.

We first note that the third of the questions raised above is not fully justified. Figure 9 shows that a GTO BS of triple-zeta plus polarization quality quite accurately reproduces the valence ED obtained with a rich PW set and using norm conserving PPs [2]. The results here reported are obtained with the PBE Hamiltonian. The effect of other choices for the exchange-correlation potential on the ED of Aluminium seems less relevant than in the case of the insulators considered in the previous sections. For instance, the value of the ED at the midpoint between two second-neighbor Al atoms is 0.0166 (0.0165); 0.0163 (0.0161); 0.0164 (0.0160) e Bohr^{-3} for PBE, LDA, HF, respectively, using the same computational conditions as in Figure 9 (data in parentheses are those obtained with CRYSTAL).

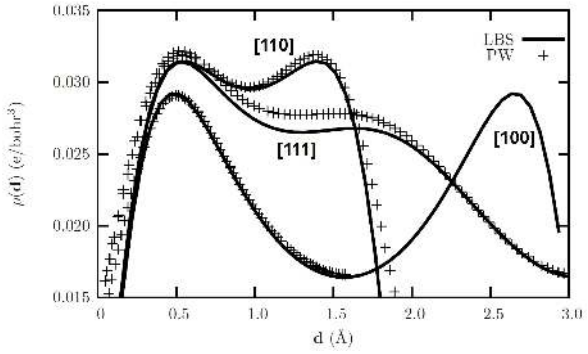

Fig. 9 Calculated valence ED of Al along the main directions using the PBE Hamiltonian. The Quantum-ESPRESSO results (crosses) were obtained using a PW cutoff of 25 Ry and a 20×20×20 grid; for the CRYSTAL calculations (continuous lines) a 5-311G** BS (LBS) and a 16×16×16 grid were adopted.

[2] `Al.pbe-rrkj.UPF` from the Quantum ESPRESSO web site.

While no accurate experimental determination of the Al ED seems to exist to compare with the present calculated results, the same is not true as concerns EMD data from directional CPs, for which very detailed experimental data and an accurate theoretical analysis exists [82, 84]. The case is more interesting here because, as stated at the beginning of this Section, the limitations of the one-electron description of metallic systems are more evident on EMD than on ED data.

As concerns the EMD, all the present one-electron calculations provide practically the same result, namely a quasi-free characterization of valence electrons, very much in line with that provided by Canney *et al.* a few years ago [83].

Figure 10 reports calculated and experimental CPs along the [111] direction; the following can be noted. The agreement with the experiment [82] of both LDA and HF results is signifi cantly improved when the Lam-Platzman correlation correction [81] is included which brings in, as expected, an increase of momentum densities just above the Fermi momentum ($K_F \approx 0.92$ a.u.), and a decrease at low momenta. Apparently, HF performs slightly better than LDA.

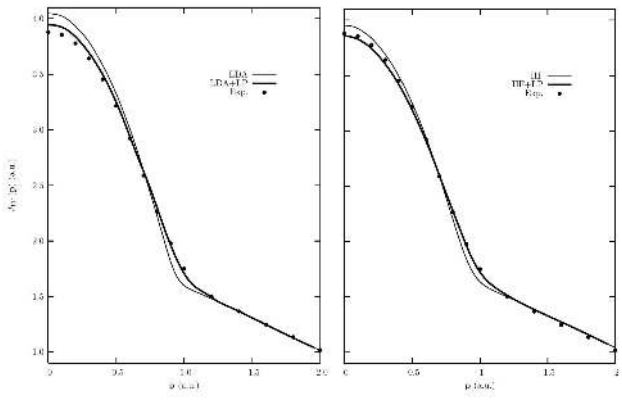

Fig. 10 CPs of Al in the [111] direction. LDA (left panel) and HF (right panel) all-electron results (thin continuous lines), were obtained with CRYSTAL using the same setup as in Figure 9; the thick continuous lines show the Lam-Platzman-corrected data. Experimental data (small full circles) are from reference [82]. All calculated data were corrected for the experimental resolution.

CP anisotropies may provide additional information on the performance of various theoretical schemes, because many systematic errors which may be present in the individual experimental CPs are cancelled when performing the difference. Figure 11 reveals non negligible differences between the two calculated anisotropies: they are however quite small, of the same order as the experimental error (± 0.02 a.u.), so nothing defi nite can be inferred in the present case.

4.4 ESD: The effect of the Hamiltonian on spin localization

An important sector of DM studies aims at the determination of accurate ESD data of spin-polarized crystals from diffraction experiments using polarized neutrons [86, 87] (see also Chapter 14). The treatment of non-collinear magnetism in solids is very

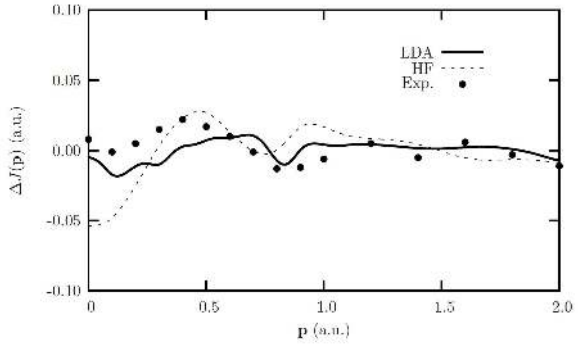

Fig. 11 CP anisotropy $[J_{110}(\mathbf{p}) - J_{111}(\mathbf{p})]$ for the Al crystal, at the HF (dotted line) and LDA (continuous line) level of theory. Experimental data (small full circles) are from reference [82].

complex, and only recently some solutions have been proposed within KS-LDA approaches [88]. In many instances, however, when the spins are essentially aligned along one preferential direction, it may be expected that a single-determinant spin-unrestricted approach can provide a satisfactory description of ESD. These cases are ideally suited to ascertain the effect the expression adopted for the corrective potential $\widetilde{V}^{\mathrm{X},\sigma}$ on the calculated ESD.

We consider here the case of a cubic perovskite ($KMnF_3$). The Mn^{+5} ions, formally in a d^5 configuration, are at the center of an octahedron of F^- ions, while K^+ ions occupy the center of the vacancies between F^- octahedra. $KMnF_3$ can be found in a ferromagnetic (FM) configuration (all spins aligned) or an antiferromagnetic (AFM) one, where spins are opposite in sign on first neighbor Mn ions. The AFM configuration is more stable, due to a super-exchange effect mediated by the F ions midway between neighboring Mn ions. The magnetic coupling constant J (calculated from the difference in stability between the two configurations with reference to the Ising Hamiltonian) is experimentally known to be -3.65 K [89].

The unrestricted (u-) results reported below were obtained with the CRYSTAL program, by trying a variety of $\widetilde{V}^{\mathrm{X},\sigma}$ expressions (see table 2), and using an all-electron BS of double-zeta quality (triple-zeta for fluorine). It is known that, while HF eccessively favors spin localization (the exact-exchange operator $\widehat{V}_{\mathrm{exch}}$ in equation 27 very effectively screens from each other electrons with the same spin), the opposite is true with expressions of the $\widetilde{V}^{\mathrm{KS}}$ potential currently used; hybrid-exchange schemes are expected to work optimally in this respect.

Figure 12 shows ESD data obtained for the FM and AFM configurations using either the HF or an LDA (SVWN) Hamiltonian. Table 4 reports ESD and J data for a variety of one-electron Hamiltonians.

The general picture is similar in all cases. Apart from a fine structure near the nuclei, a very high ESD peak is observed at about 0.4 Bohr from the Mn nucleus, and a much smaller one at about 0.3 Bohr from the F nucleus; broadly speaking, the AFM picture can be obtained by reporting, in alternating cells, the opposite of the FM ESD. On closer inspection, it is found that the height of the Mn peak decreases and that of the F peak increases, when passing from HF, to the two hybrid schemes (PBE0 and B3LYP with a fraction of 25% and 20% exact exchange,

respectively), to GGA (PBE), to LDA. This reflects the decreasing capability of localizing spin densities along this sequence. Higher values of the spin density on F entail larger super-exchange effects, which explains why the spin coupling constant is over-estimated with LDA, and under-estimated with HF. From a comparison with the experimental value of J, it can be argued that the ESD calculated with PBE0 is possibly the one closest to reality.

The alternative DFT+U scheme for favoring spin-localization in the frame of KS theory has been described in Section 3.3.2. The parallel application of the two techniques to the case of magnetic defects associated with O vacancies in metal-supported NiO and MgO monolayers has recently permitted their relative merits and problems to be analyzed [91].

	maxima of ESD/(au)				
Hamiltonian	Mn-FM	Mn-AFM	F-FM	F-AFM	J/K
u-HF	1.095	1.094	0.027	0.025	-1.251
u-PBE0	1.039	1.033	0.040	0.034	-5.659
u-B3LYP	1.036	1.028	0.048	0.039	-7.879
u-PBE	1.005	0.980	0.047	0.037	-14.103
u-SVWN	0.998	0.967	0.047	0.035	-16.384

Table 4 ESD data for $KMnF_3$. For a variety of Hamiltonians, the calculated height of the FM- and AFM-ESD maxima in the valence region of Mn and F are reported, along with the calculated value of the spin coupling constant J (in Kelvin) whose experimental value is -3.65 K.

5 Ongoing developments

The subjects dealt with below are by no means exhaustive of ongoing theoretical research in the simulation of DMs and DFs in crystals. Rather, they serve the purpose of providing an indication of promising developments intended to overcome the limitations of existing software.

5.1 The harmonic treatment of thermal effects

It has been argued in Section 3.4.1 that a rather accurate description of the nuclear motions can often be obtained in the frame of the Born-Oppenheimer separation, by adopting the harmonic approximation. Vibrational modes in a crystal (phonons) can be described in terms of displacements of atoms in the unit cell and by a Bloch vector $\mathbf{q}$ in the Brillouin Zone. These modes can be conveniently calculated at any $\mathbf{q}$ using Density-Functional Perturbation Theory, as implemented in Quantum ESPRESSO [46].

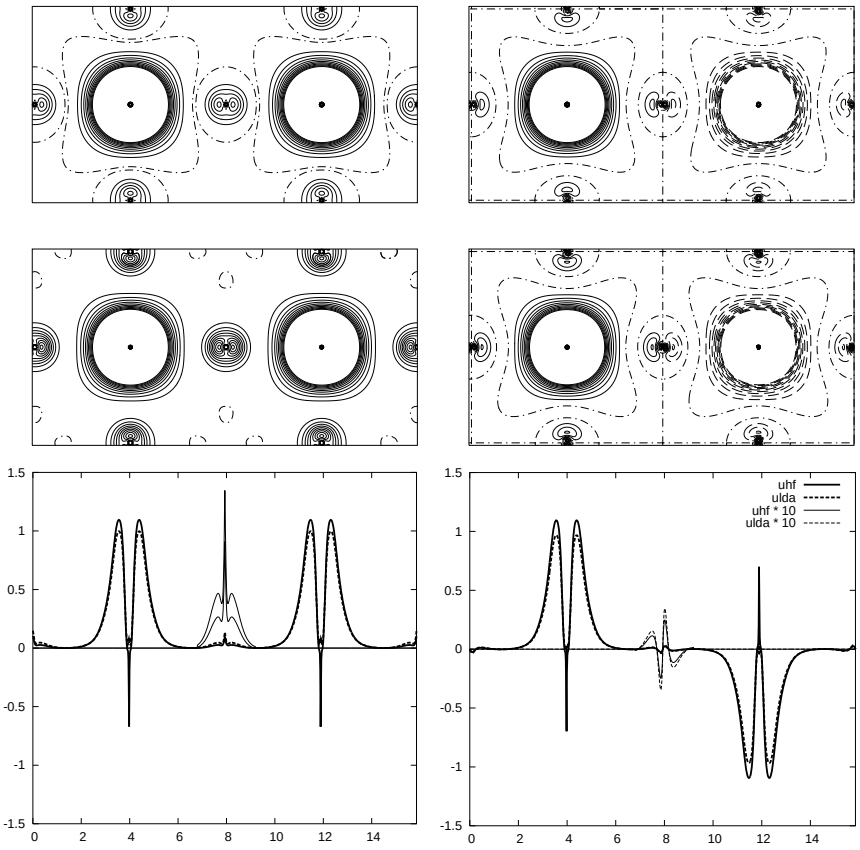

Fig. 12 ESD data for $KMnF_3$. The four plots on top are ESD maps in a plane containing Mn ions and four of their six nearest F ions, corresponding to the FM (left) and AFM (right) spin configurations, and are obtained using unrestricted HF (above) or LDA (below). Continuous, dashed and dot-dash isolines refer to positive, negative and zero ESD values, respectively; they are separated by 0.005 au; those whose value is larger than 0.05 au (near the core of Mn) are not drawn. The two bottom plots report the FM- and AFM-ESD values along the line F-Mn-F-Mn-F (the distance from the F at the left is in Bohr). HF and LDA results are drawn as a continuous and a dotted line, respectively. The thin lines near the central F ion are a blow-up of the same data in that region by a factor 10.

In the following we instead suppose that the problem has been solved by using an F-fold supercell containing $F \times M$ nuclei. This amounts to defi ning $S = 3M \times F - 3$ normal modes each characterized by a normal coordinate Q_I and a characteristic angular frequency ω_I. The general eigenfunction for the nuclei can then be obtained by assigning an excitation level $n_I = 0, 1, \ldots$ to each mode, and by multiplying by each other the S corresponding normalized eigenfunctions $H_{n_I}(Q_I)$ of the one-dimensional harmonic oscillator:

$$\Phi_{\mathbf{n}}^{\mathrm{Nuc}}(\{\mathbf{R}(\{\mathbf{Q}\})\}) = \prod_{I=1}^{S} H_{n_I}(Q_I)\ ; \tag{50}$$

the associated energy is simply given (in au) by $E_{\mathbf{n}} = \sum_I \omega_I(n_I + 1/2)$. Here $\{\mathbf{R}(\{\mathbf{Q}\})\}$ gives the position of the $F \times M$ nuclei in the supercell in terms of the set $\{\mathbf{Q}\}$ of the normal coordinates.

For a given temperature T, a Boltzmann weight $w_B(\mathbf{n}, T) = \exp(-E_{\mathbf{n}}/kT)/Z$ can be assigned to $\Phi_{\mathbf{n}}^{\mathrm{Nuc}}$. Owing to a statistical ensemble approach we can then defi ne a joint-probability density for the set of the nuclei at the temperature T:

$$\rho^{\mathrm{Nuc}}(\{\mathbf{R}\}; T) = \sum_{\mathbf{n}} w_B(\mathbf{n}, T) |\Phi_{\mathbf{n}}^{\mathrm{Nuc}}(\{\mathbf{R}\})|^2 \tag{51}$$

This function contains information on the *correlated* motion of all nuclei within the supercell. It can incidentally be noted that only the softest modes contribute signifi cantly to the probability density at $\{\mathbf{R}\}$ coordinates not too close to $\{\mathbf{R}^{\mathrm{eq}}\}$: for them, the experimental information is usually insuffi cient to verify the adequacy of the theoretical harmonic description.

If we are interested in the probability distribution for a given nucleus (the Y-th, say), we have to integrate over the coordinates of all other nuclei:

$$\rho^{\mathrm{Y}}(\mathbf{R}; T) = \int \rho^{\mathrm{Nuc}}(\{\mathbf{R}\}; T)_{\mathbf{R}_Y = \mathbf{R}}\, \mathrm{d}\{\mathbf{R}\}_{A \neq Y} \tag{52}$$

$\rho^{\mathrm{Y}}(\mathbf{R}; T)$ has the full periodicity of the lattice. It can be used in principle for calculating iso-density surfaces enclosing a certain fraction (for instance 75%) of the occurrence probability of nucleus Y, to be compared to the anisotropic displacement parameters derived from X-ray and neutron diffraction experiments (especially important for hydrogens). In fact, simpler techniques are usually adopted for this purpose, which combine semi-empirical information from diffraction data with that resulting from normal mode analysis and take only approximately into account the correlation of nuclear motions [94].

The joint nuclear probability distribution of equation (51) can be used in principle to obtain thermally averaged DFs, $\langle\langle \rho(\mathbf{y})\rangle\rangle_T$, where $\mathbf{y}$ can be $\mathbf{x}$, $\mathbf{r}$ or $\mathbf{p}$. Consider a sample of nuclear confi gurations in the supercell, $\{\mathbf{R}\}_j^T$, $(j = 1, \ldots, J)$, which has been generated so as to reflect the distribution probability $\rho^{\mathrm{Nuc}}(\{\mathbf{R}\}; T)$ (this may be accomplished, for instance, using a Metropolis algorithm [97, 98]). For each of them, the DF $\rho_j(\mathbf{y}) \equiv \rho(\mathbf{y}; \{\mathbf{R}\}_j^T)$ can be evaluated as seen in Section 2. If it is assumed that the electron distribution follows istantaneously the nuclear motion, we can write, for large J:

$$\langle\langle \rho(\mathbf{y})\rangle\rangle_T ; \approx \frac{1}{J} \sum_j \rho_j(\mathbf{y}) \tag{53}$$

While this equation seems at present exceedingly costly for practical applications, its use might be considered for benchmark studies with simple systems.

5.2 The effect of external fields

Among experimentalists, the effect of external fields on the properties of condensed matter, for instance, on their DFs is a subject of increasing interest [93]. We consider here the case where a constant electric field $\mathbf{E}$ acts on a finite (but macroscopic) crystalline sample; the field direction, $\mathbf{E}/|\mathbf{E}|$, perpendicular to the crystalline planes of Miller indices (h,k,ℓ), will be indicated conventionally as z. In the molecular case, the addition of an external potential $V^{\text{ext}} = \mathbf{E}\cdot\mathbf{r} + c$ to the Hamiltonian (2) introduces no essential complications for the solution of the corresponding problem (equation 1). The situation is different with (pseudo-)periodic systems, because the super-imposed potential destroys translational periodicity along z.

Two ways around this difficulty are implemented in CRYSTAL and in Quantum ESPRESSO. Both techniques are primarily intended to obtain the derivatives of energy with respect to the field components, which are essential for calculating the dielectric constant, the polarizability and hyperpolarizabilities of the crystal. These quantities are not only important on their own, but also because they are a necessary intermediate for evaluating the intensity of the vibrational excitations. A side benefit, however, which concerns us in the present context, is that information can be obtained on the change induced by the field on DM.

The first technique consists in superimposing to the crystal a "sawtooth" potential with periodicity D along z: $V^{\text{ext}}(z) = E\zeta$, where $\zeta = (-1)^n(z - nD/2)$ and $n = \text{int}[2z/D - 1/2]$. If $[\mathbf{a}'_1, \mathbf{a}'_2, \mathbf{a}'_3]$ is a "plane adapted" basis, with $\mathbf{a}'_1, \mathbf{a}'_2$ in the (h,k,ℓ) plane, and if D is a multiple of the interlayer distance d between those planes ($D = md$), then the crystal with unit supercell $[\mathbf{a}'_1, \mathbf{a}'_2, m\mathbf{a}'_3]$ preserves translational periodicity even in the presence of the added field, and its solution can be achieved according to the standard procedure [99]. In spite of the rather artificial device adopted (the derivative of the added potential is discontinuous at $z = nD/2 + D/4$), this technique performs surprisingly well [100] and, if m is large enough, in a region between the discontinuity planes the solution appears "quasi-periodic" with respect to translations $\mathbf{a}'_3$: this permits the changes in the DM to be analyzed by considering a cell in that region and its neighboring ones.

The second technique aims at calculating the zero-field derivatives of the energy ($\mathscr{E}_{abc\ldots}$) with respect to the field components. For this purpose, an extension to periodic systems of coupled-perturbed HF and DFT has been implemented in CRYSTAL [101, 102]. It provides first, second and third energy derivatives for systems periodic in 0, 1, 2, 3 dimensions. A by-product of these calculations are the derivatives of the DM elements in the GTO BS with respect to the field components: $\mathscr{P}_{\mu\nu|abc\ldots}$. This allows in principle the estimate of the effect of a finite (but small) field in the general (z) direction on the DM, through a truncated Taylor expansion about its unperturbed value:

$$P_{\mu\nu}(E) = P_{\mu\nu}(0) + \mathscr{P}_{\mu\nu|z}E + \frac{1}{2}\mathscr{P}_{\mu\nu|zz}E^2 + \ldots \tag{54}$$

The results with the two techniques are in excellent agreement but the second one is easier to use, more accurate and cheaper.

The recent study of the inverse piezo-electric effect in α-quartz performed with the Wien2k code [3] provides a nice example of the use of the sawtooth technique [103]: both the atomic displacements and the change of the structure factors as a function of the fi eld strength were calculated, in fair agreement with the experiment.

We fi nally remark that Quantum ESPRESSO also implements, in the framework of DFT, a third technique: fi nite macroscopic electric fi elds, treated via the modern theory of polarizability and the Berry phase concept [104, 105].

5.3 Post-HF description of DMs: the perturbative approach

In the fi eld of molecular studies, the use of post-HF techniques allows extremely accurate results to be collected, which is not possible using DFT-based schemes. While the main objective is usually the evaluation of energy eigenvalues, signifi cant information can also be obtained as concerns wave-function related properties, in particular DMs and DFs. Among the many examples, we can cite the study on the ED of bullvalene and concerning the different types of C-C bonds in this molecule [92]: it is shown that both the use of a very good BS *and* the inclusion of correlation effects (at an MP2 level) are important to bring the theoretical results to close agreement with the experimental data. The advantage over DFT approaches should be even more evident when considering the EMD and related DFs, for the reasons expressed in Sections 2.1 and 4.2. The cost of post-HF techniques in their standard formulation, which refers to the "canonical" HF COs delocalized over the whole system, ϕ_n^{HF}, scales however very rapidly with the number N of electrons, which prevents their use with "large" systems.

The *local-correlation* techniques proposed long ago by Pulay and others [106] provide a way out of this diffi culty: they use as a reference a representation of the occupied HF manifold in terms of localized orthonormal functions like the WFs in equation (33), and exploit the short-range character of the inter-electronic correlation. Based on these ideas, N-scaling formulations of some of the most popular correlation techniques have been implemented, e.g., in the MOLPRO code [107]: Møller-Plesset perturbation techniques in second (MP2) and higher orders, coupled-cluster algorithms including triple corrections, etc; very accurate correlated calculations for large molecules can thus be performed in reasonable times.

Quite recently, the CRYSCOR code has been developed [108] which implements an N_0-scaling local-correlation approach for crystals in an AO BS, though limited, for the time being, to an LMP2 level of approximation ("L" standing for "local") and to the case of spinless insulating systems. CRYSCOR uses as a reference the HF solution provided by CRYSTAL in the form of equation (34): $\left[\Psi_0^{\mathrm{HF}} = ||\ldots[\ell\mathbf{T_m}]^{\alpha}[\ell\mathbf{T_m}]^{\beta}\ldots||\right]$; in addition, CRYSTAL provides all information concerning structure, symmetry and Fock matrix of the crystal. An essential feature of CRYSCOR which permits the LMP2 solution for relatively complicated peri-

odic systems to be obtained in reasonable times, is the very efficient treatment of two-electron repulsion integrals, based on a combination of density-fitting and of multipolar techniques at short range and long range, respectively [109].

Energy related quantities are obviously the primary object of interest for such a code, since its use permits the importance of correlation effects to be estimated as concerns equilibrium geometries, elastic constants, vibrational spectra, cohesive energy, etc. However, as is clear from the preceding, DM related quantities in crystals represent a very rich ground for comparison between experiment and theory: it is therefore of interest to extract from a post-HF code also this kind of information. Two computational schemes have been implemented in CRYSCOR for this purpose, which provide an estimate $P^{(x)}(r, r')$ of the correlated DM: they can be related to the "expectation value" and the "response to an external perturbation" method, respectively, as are adopted in molecular calculations (see for example [110] and references therein).

The former technique ($x = a$) [111] defines a *locally-correlated wavefunction*, obtained by adding to the HF solution only those bi-excitations from two WFs to the unoccupied manifold where one of the two WFs is in the zero cell, but using for them the amplitudes from the periodic calculation. It can be viewed in a sense as the result of an "embedding" calculation, where electrons are allowed to correlate their motions in the zero cell and its neighborhood but are imposed to stay in their HF state far from it. There is more than that, however: for instance, the amplitudes include the effect of dispersive interactions up to infinite distance. A size-consistent periodic expression $P^{(a)}(r, r')$ can be obtained from there, which can be used for calculating the quantities of interest (ED, EMD, CPF, structure factors, etc.) by simply feeding this corrected DM instead of the HF one to the corresponding subroutines of CRYSTAL.

The second scheme ($x = b$) [112] is based on the calculation of the DM as the derivative of the LMP2 Lagrangian with respect to an external perturbation. In order to obtain a closed and simple expression, the response of the excitation amplitudes themselves to the external perturbation is not taken into account in this first implementation. An example of application of this approach has been provided in Section 4.2. Its generalization for including self-consistently orbital relaxation is the object of future work.

6 Final considerations

Present-day ab-initio computer codes for periodic systems have been shown to provide valuable information on the DM and related functions. This may help experimentalists for the analysis and interpretation of their data concerning structure factors and CPs of crystals and their dependence on external conditions. Vice-versa, the availability of high quality experimental data concerning DMs is extremely important to assess the limitations of these powerful tools.

Two issues have been here devoted special attention to in this respect.

The Hamiltonian issue. Almost all present-day calculations of the electronic structure of crystalline systems are performed using one-electron approximations (DFT, HF or hybrid). Based on practical examples, it has been argued that very accurate DM predictions can be so obtained, probably hybrid Hamiltonians providing the best results on average. Definite discrepancies from the experiment, requiring more advanced theoretical tools, seem more likely to concern EMDs, both due to recent progress in the experimental determination of directional CPs, and to the fact that the instantaneous correlation of electronic motions affects more directly their momentum that their spatial distribution.

The basis set issue. It has been shown that the quality of the representative BS is extremely important not only as concerns energy, but also densities. PWs provide a reference in this respect, especially as concerns valence electrons. Calculations based on local functions (GTFs) can approach the PW results, but only using extensive sets allowing for large flexibility and including polarization functions.

We have finally tried to get a glimpse of the exciting new developments which are expected in a near future in this area of research: they will contribute to make the experiment-theory interaction even more fruitful in years to come.

Acknowledgements The Authors are grateful to Alessio Meyer, Lorenzo Paulatto, Michele Catti, Piero Ugliengo, Marta Corno, Bartolomeo Civalleri, Mauro Ferrero for useful suggestions and for their contribution to performing some of the calculations whose results are here reported. They are also indebted to the Referees and to the Editors of this book for their most helpful remarks and comments.

References

1. P. Giannozzi, S. Baroni, N. Bonini, M. Calandra, R.Car, C. Cavazzoni, D. Ceresoli, G. L. Chiarotti, M. Cococcioni, I. Dabo, A. Dal Corso, S. Fabris, G. Fratesi, S. de Gironcoli, R. Gebauer, U. Gerstmann, C. Gougoussis, A. Kokalj, M. Lazzeri, L. Martin-Samos, N. Marzari, F. Mauri, R. Mazzarello, S. Paolini, A. Pasquarello, L. Paulatto, C. Sbraccia, S. Scandolo, G. Sclauzero, A. P. Seitsonen, A. Smogunov, P. Umari, R.M. Wentzcovitch, *J. Phys.: Condens. Matter* 21, 395502 (2009). Web site: `www.quantum-espresso.org/` .
2. R. Dovesi, V.R. Saunders, C. Roetti, R. Orlando, C.M. Zicovich-Wilson, F. Pascale, B. Civalleri, K. Doll, N.M. Harrison, I.J.Bush, Ph. D'Arco, M. Llunell *CRYSTAL06 User's Manual* (Università di Torino, Torino, 2006). Web site: `www.crystal.unito.it/` .
3. X. Gonze, J.-M. Beuken, R. Caracas, F. Detraux, M. Fuchs, G.-M. Rignanese, L. Sindic, M. Verstraete, G. Zerah, F. Jollet, M. Torrent, A. Roy, M. Mikami, Ph. Ghosez, J.-Y. Raty, D. C. Allan, *Comp. Mater. Sci.* 25, 478 (2002) [`www.abinit.org`]; G. Kresse, J. Furthmuller, *Comp. Mater. Sci.*, 6, 15 (1996) [`cmp.univie.ac.at/vasp`]; E. Artacho, E. Anglada, O. Dieguez, J.D. Gale, A. Garca, J. Junquera, R. M. Martin, P. Ordejn, J. M. Pruneda, D. Snchez-Portal, J.M. Soler, J. Phys.: Condens. Matter 20, 064208 (2008) [`www.icamb.es/siesta`]; K. Schwartz, *J. Solid State Chem.* 176, 319 (2003) [`www.wien2k.at`]; K. Koepernik and H. Eschrig, Phys. Rev. B 59, 1743 (1999) [`www.fplo.de`].

4. R. McWeeny, B.T. Sutcliffe, *Methods of Molecular Quantum Mechanics* (Academic Press, London 1969).
5. T. Kato, *Commun. Pure Appl. Math.* 10, 151 (1957).
6. P. Hohenberg, W. Kohn, *Phys. Rev.* 136, 864 (1964).
7. W. Kohn, L.J. Sham, *Phys. Rev.* 140, 1133 (1965).
8. R.F.W. Bader, *Atoms in Molecules – A Quantum Theory* (Oxford University Press, Oxford, 1990).
9. C. Gatti, *Z. Kristallogr.* 220, 399 (2005).
10. C. Gatti, in: *The Quantum Theory of Atoms in Molecules: from Solid State to DNA and Drug Design*, C.F. Matta, R.B. Boyd, Eds., Chapter 7 (Wiley-VCH Verlag, Weinheim, 2007).
11. T.S. Koritsanzsky, Ph. Coppens, *Chem. Rev.* 101, 1583-1627 (2001).
12. M. Tinkham, *Group Theory and Quantum Mechanics* (McGraw- Hill, New York, 1964).
13. T. Hahn (ed.), *International Tables for Crystallography, 3rd Revised Edition, Vol A, Section 2.13* (Kluwer, Dordrecht, 1992).
14. B. Williams (ed.), *Compton Scattering: The Investigation of Electron Momentum Distributions* (McGraw-Hill, New York, 1977).
15. R. Benesc, S.R. Singh, V.H. Smith, *Chem. Phys. Lett.* 10, 151 (1971); W. Sch¨ulke, *Phys. Status Sol. B* 82, 229 (1977); P. Pattison, W. Weyrich, B. Williams, *Solid State Commun.* 21, 967 (1977); W. Weyrich, P. Pattison, B. Williams, *Chem. Phys.* 41, 271 (1979).
16. G.E.W. Bauer, *Phys. Rev. B* 27, 5912 (1983).
17. H.J. Monkhorst, J.D. Pack, *Phys. Rev. B* 13, 5188 (1976).
18. G. H. Wannier, *Phys. Rev.* 52, 191 (1937).
19. N. Marzari, D. Vanderbilt, *Phys. Rev. B* 56, 12847 (1997).
20. C.M. Zicovich-Wilson, R. Dovesi, V.R. Saunders, *J. Chem. Phys.* 115, 9708 (2001); S. Casassa, C. Zicovich-Wilson, C. Pisani, *Theor. Chem. Acc.* 116, 726 (2006).
21. Z.W. Lu, A. Zunger, M. Deutsch, *Phys. Rev. B* 47, 9385 (1993).
22. Z. Su, P. Coppens, *Acta. Cryst. A* 54, 646 (1998); P. Macchi, P. Coppens, *Acta. Cryst. A* 57, 656 (2001).
23. J.C. Phillips, L. Kleinmann, *Phys. Rev.* 116, 287 (1959).
24. D.R. Hamann, M. Schl¨uter, C. Chiang, *Phys. Rev. Lett.* 43, 1494 (1979).
25. D. Vanderbilt, *Phys. Rev. B* 41, 7892 (1990).
    Web site: `www.physics.rutgers.edu/~dhv/uspp`.
26. P.E. Bl¨ochl, *Phys. Rev. B* 50, 17953 (1994); G. Kresse, D. Joubert, *Phys. Rev. B* 59, 1758 (1999).
27. R. Car, M. Parrinello, *Phys. Rev. Lett.* 55, 2471 (1985).
28. P. Pulay, *Mol. Phys.* 17, 197 (1969).
29. J. P. Perdew, K. Schmidt, *AIP Conf. Proc.* 577, 1 (2001).
30. J. P. Perdew, Y. Wang, *Phys. Rev. B* 45, 13244 (1992).
31. V. N. Staroverov, G. E. Scuseria, J. Tao, J. P. Perdew, *Phys. Rev. B* 69, 075102 (2004).
32. A. D. Becke, *J. Chem. Phys.* 98, 5648 (1993).
33. A. H. MacDonald, S. H. Vosko, *J. Phys. C* 12, 2977 (1979).
34. J.P. Perdew, A. Zunger *Phys. Rev. B* 23, 5048 (1981).
35. Y. Zhao, D. G. Truhlar, *J. Chem. Phys.* 128, 184109 (2008).
36. J. C. Slater, *Phys. Rev.* 81, 385 (1951).
37. S. H. Vosko, L. Wilk, M. Nusair, *Can. J. Phys.* 58, 1200 (1980).
38. J. P. Perdew, K. Burke, M. Ernzerhof, *Phys. Rev. Lett.* 77, 3865 (1996).
39. J. P. Perdew, J. Chevary, S. Vosko, K. Jackson, M. Pederson, D. Singh, C. Fiolhais, *Phys. Rev. B* 46, 6671 (1992).
40. J. P. Perdew, A. Ruzsinsky, G.I. Csonka, O.A. Vydrov, G.E. Scuseria, L.A. Constantin, X. Zhou, K. Burke, *Phys. Rev. Lett.* 100, 136406 (2008).
41. F. A. Hamprecht, A. J. Cohen, D. J. Tozer, N. C. Handy, *J. Chem. Phys.* 109, 6264 (1998).
42. Z. Wu, R. Cohen, *Phys. Rev. B* 73, 235116 (2006).
43. C. Lee, W. Yang, R. G. Parr, *Phys. Rev. B* 37, 785 (1988).
44. A. D. Becke, *Phys. Rev. A* 38, 3098 (1988).

45. R. Demichelis, B. Civalleri, M. Ferrabone, R. Dovesi, *Intern. J. Quantum Chem.*, 110, 406 (2010).
46. S. Baroni, S. de Gironcoli, A. Dal Corso, P. Giannozzi, *Rev. Mod. Phys.* 73, 515 (2001).
47. C. G. Van de Walle, P. E. Bl¨ochl, *Phys. Rev. B* 47, 4244 (1993); B. Het´enyi, F. de Angelis, P. Giannozzi, R. Car, *J. Chem. Phys.* 115, 5791 (2001).
48. V.I. Anisimov, J. Zaanen, O.K. Andersen, *J. Phys. Rev. B* 44, 943 (1991).
49. M. Cococcioni, S. de Gironcoli, *Phys. Rev. B* 71, 035105 (2005).
50. C. Pisani, R. Dovesi, *Intern. J. Quantum Chem.* 17, 501 (1980); C. Pisani, R. Dovesi, C. Roetti, *Hartree-Fock ab-initio Treatment of Crystalline Systems: Lecture Notes in Chemistry, Vol. 48* (Springer, Heidelberg, 1988).
51. E. Clementi, J. Mehl, IBMOL 5 Program User's Guide, Publication RJ889, IBM Corporation (1971).
52. D.J. Hehre, W.A. Lathan, M.D. Newton, R. Ditchfield, A. Pople, *GAUSSIAN70 Program Number 236, QCPE*, Indiana University, Bloomington, Indiana (1972).
53. M. Dupuis, D. Spangler, J. Wendoloski, NRCC Software Catalog, Vol. 1, Program No. QG01 (GAMESS) (1980).
54. Y. Noel, P. D'Arco, R. Demichelis, C.M. Zicovich-Wilson, R. Dovesi, *J. Comp. Chem.*, 31, 855 (2010).
55. C.M. Zicovich-Wilson, F.J. Torres, F. Pascale, L. Valenzano, R. Orlando, R. Dovesi, *J. Comp. Chem.* 29, 2268 (2008).
56. C. Gatti, TOPOND-98 User's manual, CNR-CSRSRC, Milano, Italy (1999). Web site: `www.istm.cnr.it/~gatti/` .
57. H.-J. Werner, P. Knowles, F. Manby, *J. Chem. Phys.* 118, 8149 (2003).
58. T.H. Dunning, *J. Phys. Chem.* A104, 9062 (2000).
59. F. Jensen, *J. Chem. Phys.* 110, 6601 (1999).
60. S.F. Boys, F. Bernardi, *Mol. Phys.* 19, 553 (1970).
61. N.R. Kestner, J.E. Combariza, *Rev. Comp. Chem.* 13, 99 (1999).
62. R. Dovesi, C. Pisani, F.Ricca, C. Roetti, V.R. Saunders, *Phys. Rev. B* 30, 972 (1984); M. Causà, R. Dovesi, C. Pisani, C. Roetti, *Phys. Rev. B* 32, 1196 (1985).
63. M. Causà, R. Dovesi, C. Pisani, C. Roetti, *Acta Cryts. B* 42, 247 (1986); M. Causà, R. Dovesi, C. Pisani, C. Roetti, *Phys. Rev. B* 34, 2939 (1986).
64. E. Nishibori, E. Sunaoshi, A. Yoshida, S. Aoyagi, K. Kato, M. Takata, M. Sakata, *Acta. Cryst. A* 63, 43 (2007).
65. R. Orlando, R. Dovesi, R. Orlando, C. Roetti, V.R. Saunders, *J. Phys. C: Condens. Matter* 2, 7769 (1990).
66. C. Pisani, R. Dovesi, R. Orlando, *Intern. J. Quantum Chem.* 42, 5 (1992).
67. H. Birkedal, D. Madsen, R.H. Mathiesen, K. Knudsen, H.-P. Weber, P. Pattison, D. Schwarzenbach, *Acta Crystall. A* 60, 371 (2004).
68. C. Gatti, V.R. Saunders, C. Roetti, *J. Chem. Phys.* 101, 10686 (1997).
69. M.A. Spackman, P.G. Byrom, M. Alfredsson, K. Hermansson, *Acta Crystall. A* 55, 30 (1999).
70. A. Erba, C. Pisani, S. Casassa, L. Maschio, M. Sch¨utz, D. Usvyat, *Phys. Rev. B*, submitted (2009).
71. S. Swaminathan, B.M. Craven, M.A. Spackman, R.F. Stewart, *Acta Crystall. B* 40, 398 (1984).
72. B. Civalleri, K. Doll, C.M. Zicovich-Wilson, *J. Phys. Chem.* 111, 26 (2007).
73. B. Civalleri, M. Ferrero, R. Dovesi (private communication).
74. A. Sch¨afer, H. Horn, R. Ahlrichs, *J. Chem. Phys.* 97, 2571 (1992).
75. V.E. Zavodnik, A.i. Stash, V.G. Tsirelson, R.Y. de Vries, D. Feil, *Acta Crystall. B* 55, 45 (1999).
76. A. Shukla, E.D. Isaacs, D.R. Hamann, P.M. Platzman, *Phys. Rev. B* 64, 052101 (2001).
77. S. Ragot, *J. Chem. Phys.* 125, 014106 (2006).
78. A. J. Thakkar, in *Theory and Applications of Computational Chemistry: The First 40 Years*, C.E. Dykstra, G. Frenking, K.S. Kim, G.E. Scuseria, Eds. (Elsevier: Amsterdam, 2005).
79. S. Raimes, *The Wave Mechanics of Electrons in Metals* (North Holland, Amsterdam, 1961).

80. S.I. Lundqvist, C. Lyd´en, *Phys. Rev. B* 4, 3360 (1971).
81. L. Lam, P. Platzman, *Phys. Rev. B* 9, 5122 (1974).
82. D.A. Cardwell, M.J.Cooper, *Phil. Mag. B* 54, 37 (1986).
83. S.A. Canney, M. Vos, A.S. Kheifets, N. Clisby, I.E. McCarthy, E. Weigold, *J. Phys.: Condens. Matter* 9, 1931 (1997).
84. D.A. Cardwell, M.J.Cooper, *J. Phys.: Condens. Matter* 1, 9357 (1989).
85. O. Aikala, T. Paakkari, S. Manninen, *Acta Crystall. A* 38, 155 (1982).
86. S.W. Lovesey, *Theory of neutron scattering from condensed matter*, Vol. I, II (Clarendon Press, Oxford, 1984).
87. G. Rousse, J. Rodr´ıguez-Carvajal, C. Wurm, C. Masquelier, *Chem. Mater.* 13, 4527 (2001).
88. H. Yamagami, *Phys. Rev. B* 61, 6246 (1999); D. Hobbs, G. Kresse, J. Hafner, *Phys. Rev. B* 62, 11556 (2000); R. Gebauer, S. Baroni, *Phys. Rev. B* 61, R6459 (2000); R. Lakowski, G.K.H. Madsen, P. Blaha, K. Schwarz, *Phys. Rev. B* 69, 140408 (2004); A. Dal Corso, A. Mosca Conte, *Phys. Rev. B* 71, 115106 (2005); A. Mosca Conte, SISSA/ISAS PhD Thesis, `www.sissa.it/cm/thesis/2007/moscaconte.pdf` .
89. L.J. de Jongh, R. Block, *Physica B* 79, 568 (1975).
90. S.L. Dudarev, A.P. Sutton, G.A.D. Briggs, *Phys. Rev. B* 55, 7859 (1997).
91. A.M. Ferrari, C. Pisani, F. Cinquini, L. Giordano, G. Pacchioni, *J. Chem. Phys.* 127, !74711 (2007).
92. T.S. Koritsanzsky, J. Buschmann, P. Luger, *J. Phys. Chem.* 100, 10547 (1996).
93. U. Pietsch, *Phys. Rev. B* 66, 155430 (2002).
94. A.E. Whitten, M.A. Spackman, *Acta Crystall. B* 62, 875 (2006);
95. A.Ø. Madsen, *J. Appl. Crystall.* 39, 757 (2006);
96. P. Munshi, A.Ø. Madsen, M.A. Spackman, S. Larsen, R. Destro, *Acta Crystall. A* 64, 465 (2008).
97. N. Metropolis, A. Rosenbluth, M. Rosenbluth, A. Teller, E. Teller, *J. Chem. Phys.* 21, 1087 (1953).
98. S.E. Koonin, D.C. Meredith *Computational Physics - Fortran version* (Addison Wesley, Reading, Mass., 1990), Chapter 8.
99. C. Darrigan, M. R´erat, G. Mallia, R. Dovesi, *J. Comp. Chem.* 24, 1305 (2003).
100. M. R´erat, M. Ferrero, R. Dovesi, *J. Comp. Meth. Sc. Eng.* 6, 233 (2006).
101. M. Ferrero, M. R´erat, B. Kirtman, R. Dovesi, *J. Chem. Phys.* 129, 244110 (2008).
102. M. Ferrero, M. R´erat, R. Orlando, R. Dovesi, *J. Comp. Chem.* 29, 1450 (2008).
103. V. Kochin, J. Davaasambuu, U. Pietsch, K. Schwarz, P. Blaha, *J. Phys. Chem. Sol.* 65, 1967 (2004).
104. I. Souza, J. Íñiguez, D. Vanderbilt, *Phys. Rev. Lett.* 89, 117602 (2002).
105. P. Umari, A. Pasquarello, *Phys. Rev. Lett.* 89, 157602 (2002).
106. P. Pulay, *Chem. Phys. Letters* 100, (1983) 151 (1983); P. Pulay, S. Saebø, W. Meyer *J. Chem. Phys.* 8, 1901 (1984); S. Saebø, P. Pulay, *Chem. Phys. Lett.* 113, (1985) 13 (1985).
107. H.-J. Werner, P.J. Knowles, R. Lindh, F.R. Manby, M. Sch¨utz and others, *MOLPRO version 2006.1, a package of ab initio programs*. Web site: `www.molpro.net`.
108. C. Pisani, L. Maschio, S. Casassa, M. Halo, M. Sch¨utz, D. Usvyat, *J. Comp. Chem.* 29, 2113 (2008). Web site: `www.CRYSCOR.unito.it`.
109. L. Maschio, D. Usvyat, *Phys. Rev. B* 78, 73102 (2008).
110. K.B. Wiberg, C.M. Hadad, T.J. LePage, C.M. Breneman, M.J. Frisch, *J. Phys. Chem.* 96, 671 (1992).
111. C. Pisani, S. Casassa, L. Maschio, *Z. Phys. Chem.* 220, 913 (2006).
112. D. Usvyat, M. Sch¨utz, *J. Phys.: Conf. Ser.* 117, 012027 (2008).

Appendix: Atomic units, Glossary of Abbreviations

Table 5 Atomic Units (au).

Quantity	Atomic unit	SI Equivalent	Notes
Mass	m_0	$9.1096\,10^{-31}$ kg	The rest mass of the electron
Charge	e	$1.6022\,10^{-18}$ C	The elementary charge
Angular Momentum	$\bar{h} = h/(2\pi)$	$1.0546\,10^{-34}$ J s	The reduced Planck constant: angular momentum operators have integer or semi-integer eigenvalues in au's
Length	$a_0 = 4\pi\,\varepsilon_0\,\bar{h}^2/(m_0\,e^2)$	$5.2918\,10^{-11}$ m	The Bohr radius of H (also called "Bohr")
Permittivity	$4\pi\varepsilon_0$	$1.1126\,10^{-10}$ $C^2m^{-1}J^{-1}$	The vacuum permittivity
Energy	$e^4 m_0/(4\pi\,\varepsilon_0\,\bar{h}^2) = 1$ E_h	$4.3598\,10^{-18}$ J	The electrostatic repulsion energy between two electrons separated by 1 a_0 (also called "Hartree", abbreviated E_h: 1 E_h=2 Ry=2625.9 kJ/mol=27.21 eV)
Speed	$e^2/(4\pi\,\varepsilon_0\,\bar{h}) = c\alpha$	$2.1877\,10^{6}$ m s^{-1}	The speed of the electron in the ground state of Bohr's H atom; c is the speed of light in vacuum, $\alpha = 137.036^{-1}$ the fine structure constant
Time	$\bar{h}/E_h$	$2.4189\,10^{-17}$ s	The time taken to travel 1 a_0 at 1 au speed
E(S)D	$1/a_0^3$	$6.7482\,10^{30}$ m^{-3}	N. of (unpaired) electrons per unit volume
EMD	$m_0\,c\alpha/a_0^3$	$1.3449\,10^{7}$ kg $m^{-2}s^{-1}$	Electron Momentum Density

Table 6 Glossary of Abbreviations

Acronym(s)	Meaning	Introduced in Section:
AE	All-Electron	2.2.3
AO	Atomic Orbital	1
BF	Bloch Function	2.2.1
BS	Basis Set	1
BSSE	Basis Set Superposition Error	3.4.2
BvK	Born-vonKarman (cyclic conditions)	2
BZ	Brillouin Zone	2.2.1
CO,CSO	Crystalline (Spin-)Orbitals	2.2
CP,CPF	Compton Profile (Function)	2.1.2
DF	Density Function (charge, spin or momentum density)	1
DFT	Density Functional Theory	2.1.1
DM	Density Matrix	1
ED,ESD	Electron Density, Electron Spin Density	2.1
EMD	Electron Momentum Density	2.1
ESD	Electron (net) Spin Density along z	2.1
FT,FFT	Fourier Transform, Fast Fourier Transformation	2.1,3.1
HF,UHF	Hartree-Fock, Unrestricted Hartree-Fock	1,2.2
GTO	Gaussian Type Orbital	3.1,3.4.2
KS,UKS	Kohn-Sham, Unrestricted Kohn-Sham	1,2.2
LMP2	Local Møller Plesset perturbation theory at order 2	5.3
MO,MSO	Molecular (Spin-)Orbitals	2.2
PAW	Projected Augmented Waves	2.2.3,3.3.1
PP	Pseudo-Potential	2.2.3
PW	Plane-Wave	1
RFF	Reciprocal Form Factor	2.1.2
USPP	Ultra-Soft Pseudo-Potential	2.2.3
WF	Wannier Function	2.2.1